Experimental Thermal and Fluid Science 36 (2012) 126–142

Contents lists available at SciVerse ScienceDirect

Experimental Thermal and Fluid Science

journal homepage: www.elsevier.com/locate/etfs

A study of discrepancies in flow boiling results in small to microdiameter metallic tubes

Tassos G. Karayiannis *, Mohamed M. Mahmoud, David B.R. Kenning

School of Engineering and Design, Brunel University, Uxbridge, London, UK

ARTICLE INFO

Article history:
Received 19 May 2011
Received in revised form 12 September 2011
Accepted 12 September 2011
Available online 19 September 2011

Keywords:
Flow boiling
Small and microtubes
Surface characteristics
Heated length

ABSTRACT

There is a disagreement in the reports on flow boiling heat transfer on the dependence of the local heat transfer coefficient on local vapour quality, mass and heat flux and system pressure. As a consequence, various conclusions were reported about the dominant heat transfer mechanism(s) in small to microdiameter tubes. Yet, the reasons behind this large disagreement are not clear. The current study investigated experimentally two important parameters that may contribute in explaining the scatter in the published heat transfer results. The first parameter is the tube inner surface characteristics and the second is the length of the heated section. The surface effect was experimentally investigated through examining two stainless steel tubes manufactured by two different methods. The first tube is a seamless cold drawn tube whilst the second is a welded tube. The two tubes have similar design and dimensions and were investigated at 8 bar system pressure and 300 kg/m^2 s mass flux. The inner surface of the two tubes was examined using a scanning electron microscope (SEM) and was found to be completely different. The heat transfer results demonstrated that the trend of the local heat transfer coefficient versus local vapour quality in the seamless cold drawn tube is completely different from that in the welded tube. Three heated lengths were investigated for a seamless cold drawn tube with an inner diameter of 1.1 mm over a wide range of experimental conditions; mass flux range of 200–500 kg/m^2 s, system pressure of 6–10 bar, inlet sub-cooling value of about 5 K and exit quality up to about 0.95. The results indicated that the heated length influences strongly the magnitude as well as the local behaviour of the heat transfer coefficient. There is a progression from nucleate boiling to convective boiling as the heated length increases. The variation in the heat transfer coefficient due to differences in the heated length may also influence the performance of the existing microscale heat transfer correlations. The flow patterns observed at the exit of each test section are also presented.

1. Introduction

In the last decade, more research was directed towards investigating flow boiling phenomena in microchannel heat exchangers. This was motivated by the urgent need for microevaporators and condensers for a wide range of applications. These include cooling high and ultra-high heat flux systems, e.g. electronic components and high power devices. For electronics cooling, flow boiling provides a superb solution compared to the other cooling techniques, e.g. fan cooling, single phase liquid cooling, jet impingement and heat pipes. It has the advantage of achieving very high heat transfer rates, using a small liquid inventory and resulting in a uniform hot surface temperature (at values slightly above the saturation temperature). Additionally, due to phase change, the temperature of the hot surface (e.g. electronic chip) does not vary significantly with the applied load (increasing or decreasing heat flux), which would not be the case if single phase forced convective cooling is used. This is very significant because it can mitigate the thermal fatigue in the chip and consequently prolong its lifetime. Other applications of mini or microheat exchangers include domestic refrigeration and air conditioning systems motivated by environmental concerns that demand new systems with high coefficient of performance (COP) and low refrigerant charge as reported in [1–3]. Despite the aforementioned advantages and applications, there are several limitations that may impede the commercial wide use of these microheat exchangers. The limitations include: (i) Possible high pressure drop; (ii) local pressure fluctuations that influence the local saturation temperature and thus the local heat transfer rates; (iii) flow instability, which in most cases is accompanied with deterioration in the heat transfer process; (iv) difficulty in triggering boiling (very high wall superheat is required). This is not desirable in electronics where it might shorten the lifetime of the chip due to working at very high temperatures before boiling incipience; (v) lack of flow boiling fundamental knowledge and thus accurate prediction correlations. All of these limitations

* Corresponding author.
E-mail address: tassos.karayiannis@brunel.ac.uk (T.G. Karayiannis).

0894-1777/$ - see front matter © 2011 Elsevier Inc. All rights reserved.
doi:10.1016/j.expthermflusci.2011.09.005

call for more research to understand the complex physics of the flow boiling phenomena in microsystems.

Examining the open literature, one can conclude that there is a disagreement on the effect of heat flux, mass flux and vapour quality on the local flow boiling heat transfer coefficient. The different trends of the local heat transfer coefficient versus local vapour quality resulted in different conclusions about the dominant heat transfer mechanism(s). A group of researchers such as [4–7] concluded nucleate boiling as a dominant heat transfer mechanism, even up to vapour quality values of about 0.8. A second group such as [8–13] reported nucleate-convective boiling mechanism, i.e. nucleation at low qualities and convection at high qualities. On the contrary, Tran et al. [14] reported convective-nucleate boiling mechanism, i.e. convection at low quality and nucleation at high quality. A third group of researchers such as [15–18] reported nucleate boiling mechanism in the region before the occurrence of dryout.

It is worth mentioning that all of the above studies investigated flow boiling in single tubes but the test fluids were different. In fact, it is very difficult to find two studies with exactly similar experimental conditions for the purpose of a good comparison. In preparing reference [19], the present authors reviewed the topic of surface effects on flow boiling heat transfer and also reviewed the experimental studies that were conducted at approximately similar conditions. Their review indicated that there is a very limited number of studies that examined the surface effects on flow boiling heat transfer (one study) and only three studies used R134a and almost the same tube diameter. Accordingly, part of the work published in [19] is included here to offer the reader a complete picture. In the following paragraphs, we will present some examples of experimental studies that used R134a as a test fluid and stainless steel tubes with approximately similar inner diameter. Tube orientation may be (approximately) ignored in the comparison due to the strong effect of surface tension.

Fig. 1 presents one example for the local heat transfer coefficient versus local vapour quality at different heat fluxes measured by three different labs for R134a and $D \approx 2$ mm. Fig. 1a depicts the results of Huo et al. [15] for a vertical stainless steel tube with an inner diameter of 2.01 mm and heated length of 211 mm at $G = 300$ kg/m^2 s and $p = 8$ bar. The results indicated that the local heat transfer coefficient increases with increasing heat flux in the region before the occurrence of dryout ($x < 0.2$–0.3) with a little dependence on vapour quality. In their study, the mass flux effect was found to be insignificant whilst increasing system pressure from 8 to 12 bar resulted in a significant increase in the heat transfer coefficient. Based on that, they proposed nucleate boiling as a dominant heat transfer mechanism before dryout. Fig. 1b depicts the results of Owhaib et al. [20] for a vertical stainless steel tube with an inner diameter of 1.7 mm and 220 mm heated length at 8.6 bar system pressure and unspecified mass flux. It indicates that the behaviour of the local heat transfer coefficient is different compared to that of Huo et al. [15] shown in Fig. 1a although the heated length is almost the same. It shows that there is a heat flux effect but the dependence on vapour quality seems unclear. The mass flux effect was found to be very small and the heat transfer coefficient increases with increasing system pressure from 6.5 to 8.6 bar. The authors suggested nucleate boiling as a dominant mechanism for $x < 0.6$. Recently, Tibirica and Ribatski [21] investigated flow boiling of R134a (also R245fa) in a horizontal stainless steel tube with an inner diameter of 2.32 mm and heated length of 464 mm. The local heat transfer coefficient was the averaged circumferential heat transfer coefficient, i.e. at each axial location the coefficient was measured at the top, bottom and the side and the average was based on the reading of three different thermocouples. The heat transfer coefficient was found to increase with increasing heat flux and vapour quality as seen in Fig. 1c. It is worth mentioning that, dryout occurred at vapour qualities greater than about 0.9, which is different compared to the result of Huo et al. [15] – note the difference in the heat flux values. System pressure was found to affect the heat transfer coefficient only at

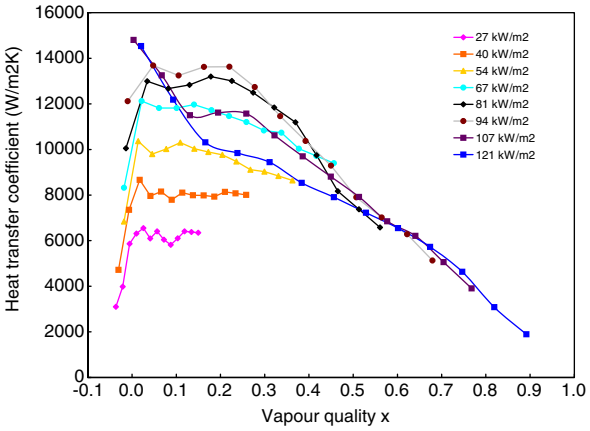

(a) D = 2.01 mm, G = 300 kg/m^2 s, P = 8 bar and L = 211 mm, [15].

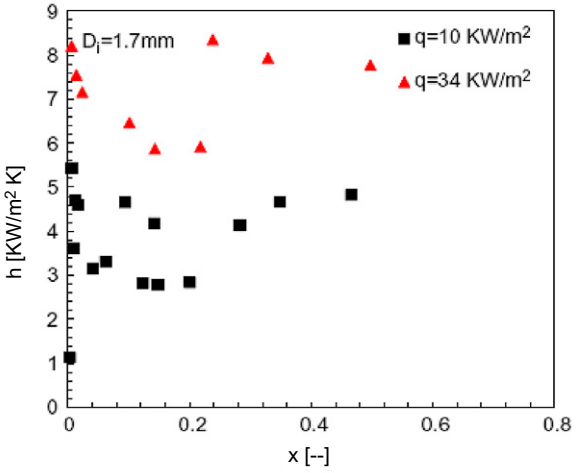

(b) D = 1.7 mm, unspecified G, P = 8.6 bar and L = 220 mm, [17].

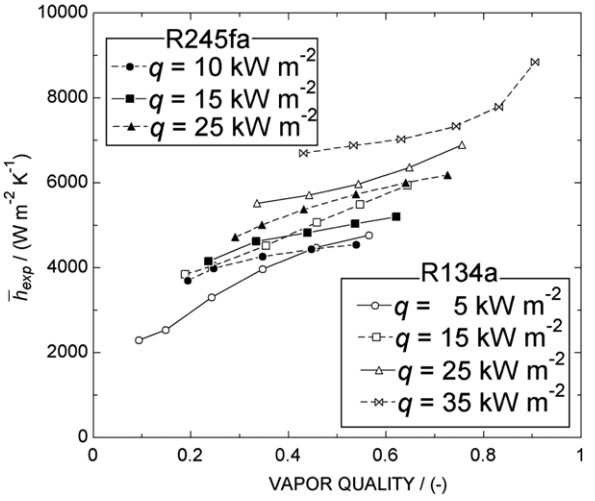

(c) D = 2.3 mm, G = 400 kg/m^2 s, P = 8 bar and L = 464 mm, [21].

Fig. 1. The effect of heat flux on the local flow boiling heat transfer coefficient as a function of local vapour quality for $D \approx 2$ mm and R134a.

low mass fluxes ($G < 300$ kg/m^2 s) and at low vapour quality values ($x < 0.55$) for the range of 6–8 bar whilst the effect was insignificant when the pressure increased from about 8 to 10 bar. A clear mass flux effect was found where the heat transfer coefficient increased with increasing mass flux within a vapour quality range of about 0.2–0.9 (no data presented for $x < 0.2$). The authors did not comment on the dominant heat transfer mechanism(s) but in their discussion they interpreted the heat flux effect using the Thome et al. [22] model. The model indicates, without considering nucleation (only film evaporation), that the heat transfer coefficient increases with increasing heat flux. It is worth mentioning that stratification effects were very clear in their experiment, where the measured heat transfer coefficient at top locations was higher than that at bottom and side locations.

A second example of the scatter in the local heat transfer behaviour is shown in Fig. 2 for $D \approx 0.5$ mm, which was presented first in reference [19]. The figure demonstrates that there is no complete agreement on the trend of the local heat transfer coefficient at different heat fluxes. In the study of Martin-Callizo et al. [17], the heat transfer coefficient increased with heat flux and exhibited a fluctuating trend with local vapour quality before the occurrence of dryout at high heat fluxes. Increasing system pressure resulted in an increase in the heat transfer coefficient whilst the mass flux effect was insignificant for $x < 0.5$. They did not comment on the dominant mechanism but conventionally their results indicate that nucleate boiling dominates for $x < 0.5$. In the study of Consolini and Thome [23], the heat transfer coefficient decreased slightly with quality up to the second thermocouple location then it increased slightly with quality towards the tube exit before it decreases at the last thermocouple location. It is also clear that the drop in the heat transfer coefficient at the last thermocouple location occurred for all heat fluxes, i.e. even at the lowest heat flux. The authors concluded that the heat transfer coefficient depends strongly on heat flux with little dependence on vapour quality and the effect of mass flux was insignificant. They did not comment on the dominant heat transfer mechanism. Contrary to these two studies, Mahmoud et al. [12] found that the heat transfer coefficient decreases greatly from its highest value at quality of about zero then it remains approximately constant for most heat fluxes over a narrow range of local vapour qualities then the lines merged into one curve showing increasing trend with increasing vapour quality. Also, the heat transfer coefficient increased with increasing mass flux for $x > 0.4$. They concluded that nucleate boiling could dominate up to $x \approx 0.4$ then convective boiling becomes the dominant mechanism. A third example for the difference in the trends of the local heat transfer coefficient versus vapour quality is clear from the experimental studies of Owhaib et al. [20], Shiferaw et al. [24] and Ong and Thome [25] for $D \approx 1$ mm. Similar conclusions to the above 0.5 mm tube can be drawn from these studies where completely different trends were reported. The reasons behind this discrepancy are not yet clear and some possible reasons are discussed in the following paragraphs.

The first reason could be flow instability, which was suggested by Consolini and Thome [23]. Most researchers presented their heat transfer results without reporting whether they correspond to stable boiling or not. In stable boiling, there is a possibility for the liquid film to continue to wet the channel wall, even at high vapour quality values. This may result in a delay in dryout to very high vapour quality values. Also it may cause the local heat transfer coefficient to increase with increasing quality in the high quality region, due to the stable film evaporation. On the contrary, in unstable boiling, the local wall temperature and consequently the local heat transfer coefficient undergo high fluctuations. Therefore, the local time averaged heat transfer coefficient may exhibit a fluctuating trend with local vapour quality. Additionally, the liquid film may be ruptured due to the high instability and therefore dryout may occur at low vapour quality values. Few researchers [23,26] presented flow boiling heat transfer results for stable and unstable boiling. They investigated flow boiling in tubes having an inner diameter of 0.51 and 0.79 mm, respectively. Their results indicated that flow boiling instability affects significantly the trend of the local heat transfer coefficient versus local vapour quality. In stable boiling, the coefficient exhibited an increasing trend with local vapour quality in the high quality region whilst it does not change significantly in case of unstable boiling. It is worth mentioning that, in the study of Consolini and Thome [23], the effect of flow instability on the heat transfer coefficient was very clear only for R236fa and R245fa whilst R134a was insensitive to flow instability although the instability conditions were the same (wall temperature fluctuations of about ±2 K). They did not comment on this result.

The second possible reason could be the difference in the inner surface characteristics, which may result from the difference in the manufacturing process (seamless versus welded tubes). Most researchers who conducted flow boiling studies in metallic tubes did not report any information about the manufacturing process or the microstructure of the inner surface of the test tubes. It is well known that the surface finish influences significantly the nucleate pool boiling heat transfer characteristics as reported recently by [27,28]. Very few studies [29,30] investigated the effect of surface roughness on flow boiling heat transfer in rectangular channels and reported a significant effect. Kandlikar and Spiesman [29] investigated the effect of surface finish on flow boiling heat transfer of sub-cooled water in a channel of 3×40 mm cross section. The channel, which was horizontal, had a rod heater inserted vertically such that the top surface of the heater formed the bottom surface of the channel. Four rod heaters of 10 mm diameter made of aluminium provided a base with different surface characteristics. The same authors reported that, for a given heat flux, variations in wall superheat up to 30% resulted when using the four heaters. Recently, Jones and Garimella [30] investigated the effect of surface roughness on flow boiling heat transfer and pressure drop of water flow in microchannels that were heated only from the bottom. The channels were fabricated from an oxygen free copper block and each channel has a cross section of 0.5×0.5 mm and 25.4 mm length. Three test pieces with different surface roughness were investigated. The first piece was fabricated by a saw blade (resulting in an average roughness value of 1.4 μm) whilst the other two pieces were roughened using electrical discharge machining (EDM) resulting in average roughness values of 3.9 and 6.7 μm. It was found that, surface roughness does not have a significant effect on the boiling incipience wall superheat and the critical heat flux. For heat fluxes less than 700 kW/m^2, surface roughness was found to have a very small effect on the saturated boiling heat transfer coefficient. However, for heat fluxes higher than this value, the roughest surfaces (3.9 and 6.7 μm) resulted in higher heat transfer coefficients compared to the smooth one (1.4 μm). For heat fluxes greater than 1500 kW/m^2, the heat transfer coefficient was 20–35% higher in the rougher surfaces compared to the smooth one. Based on the study of Kandlikar and Spiesman [29] and the study of Jones and Garimella [30], the variation in heat transfer coefficient due to surface roughness may be one of the reasons behind the scatter in the flow boiling heat transfer data. It is worth mentioning that, not only the surface roughness (average roughness) influences the nucleation process in flow boiling but also the shape of the roughness element.

A third possible reason could be the variation in the investigated heated length from one study to another. In the three experimental studies presented in Fig. 2, as an example, the heated length was different. The heated length in the study of Martin-Callizo et al. [17] was 213 mm, 78 mm in the study of Consolini and Thome [23] and 100 mm in the study of Mahmoud et al. [12].

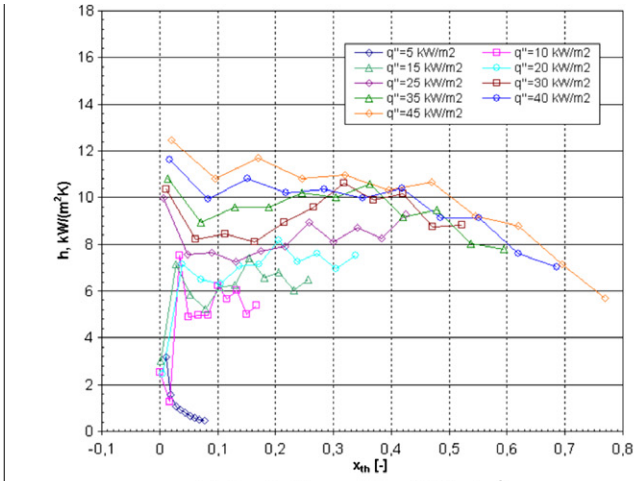

(a) D = 0.64 mm, G = 400 kg/m^2 s, P = 8.6 bar and L = 213 mm, [17].

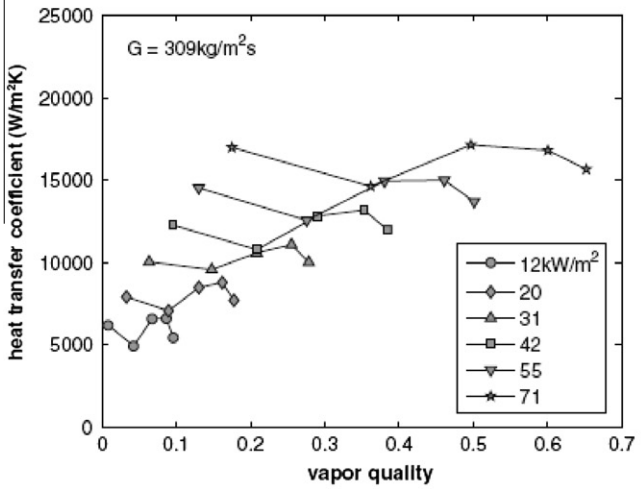

(b) D = 0.51 mm, P = 8 bar and L = 79 mm, [23].

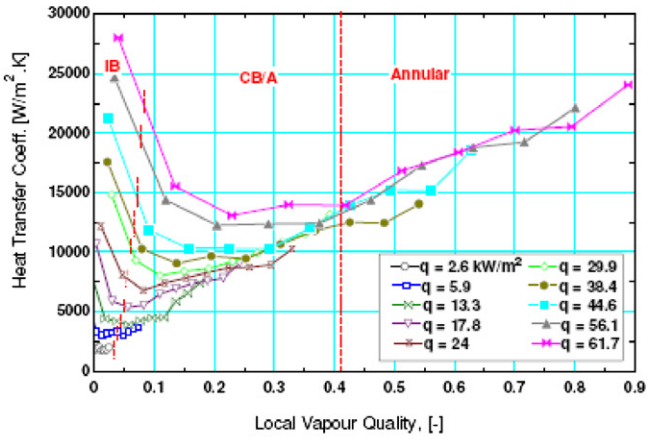

(c) D = 0.52 mm, G = 280 kg/m^2 s, P = 6 bar and L = 100 mm, [12].

Fig. 2. The effect of heat flux on the local flow boiling heat transfer coefficient as a function of local vapour quality for $D \approx 0.5$ mm and R134a.

Saitoh et al. [31] investigated a 0.51 mm diameter tube with a 550 mm heated length, which is much longer than the studies above. Conducting the test in very long tubes, for a given mass flux, will result in operation at lower heat fluxes (smaller wall superheat) and consequently the contribution of nucleate boiling may decrease. Also, the flow patterns may keep developing along the channel, which might influence the local heat transfer behaviour. On the other hand, conducting the test in very short tubes allows for the operation at high heat fluxes (high wall superheat) and consequently nucleate boiling may seem to dominate.

Some researchers [32,33] investigated flow boiling patterns of R134a in vertical tubes having an inner diameter of about 1 mm, as in the present study. Chen et al. [32] investigated flow boiling patterns of R134a in a wide range of tube diameters (1.1–4.26 mm) and identified seven flow patterns: dispersed bubble, bubbly, confined bubble, slug, churn, annular and mist flow. The confined bubble regime established in the 1.1 mm tube at all experimental conditions whereas the mist flow appeared only in the largest tube (4.26 mm). In their study, the flow patterns were observed at the exit of the heated section. Recently, Martin-callizo et al. [33] conducted a flow visualization study for R134a in a 1.33 mm diameter tube. The flow patterns were visualized in a quartz tube which was directly heated through coating the outer surface with a thin layer of Indium Tin Oxide. They observed seven flow regimes: isolated bubble, confined bubble, slug, churn, slug-annular (at the lowest mass flux value of 100 kg/m^2 s), annular and mist flow. It is worth mentioning that, in the study of Chen et al. [32], the confined bubble regime was characterized as bubbles with a smooth liquid vapour interface, same diameter as the tube and length greater than tube diameter. On the contrary, Martin-Callizo et al. [33] identified the confined bubble regime as a cap-bubbly flow (irregular shape) with diameter almost equal the tube diameter. However, these two studies demonstrate a good agreement on the observed flow patterns.

This paper extends the work presented recently in [19] on the effect of surface characteristics on the local and average heat transfer coefficient using two stainless steel tubes of similar dimensions. The two tubes have 150 mm heated length and manufactured by two different processes; cold drawn (D = 1.1 mm) and welding (D = 1.16 mm). The additional work presented in this paper relates to the effect of the heated length on the heat transfer rates using three cold drawn stainless steel tubes of different heated lengths. The experimental conditions include mass flux range of 200–500 kg/m^2 s, pressure range of 6–10 bar, exit quality up to about 0.95 and inlet sub-cooling of about 5 K.

2. Experimental facility

The experimental facility used in this study was described earlier in [15] and hence only a brief summary is given here. It consists of three main systems, i.e. the R134a main circuit, data acquisition and control, and the R22 cooling system. Fig. 3 depicts the schematic drawing of the R134a main circuit. In the tests described in this paper, four stainless steel tubes were investigated as summarized in Table 1. The welded tube (manufactured by welding process and supplied by Coopers Needle Ltd.) was included to investigate the effect of inner surface characteristics in comparison with a seamless cold drawn tube (supplied by Oxford Instruments) that has a similar heated length (L = 150 mm). The three seamless cold drawn tubes in Table 1 were used to investigate the effect of varying the heated length. Each test section consists of an adiabatic calming section with a length of 150 mm, heated section with different lengths, mentioned in Table 1 and a borosilicate visualization section with a length of 100 mm. The heated section was directly heated by passing a DC current through two copper electrodes that were welded at the inlet and outlet. The supplied power was measured directly between the test section electrodes using a Yokogawa power meter WT110 with an accuracy of ±0.29%. This was to exclude the voltage drop across the

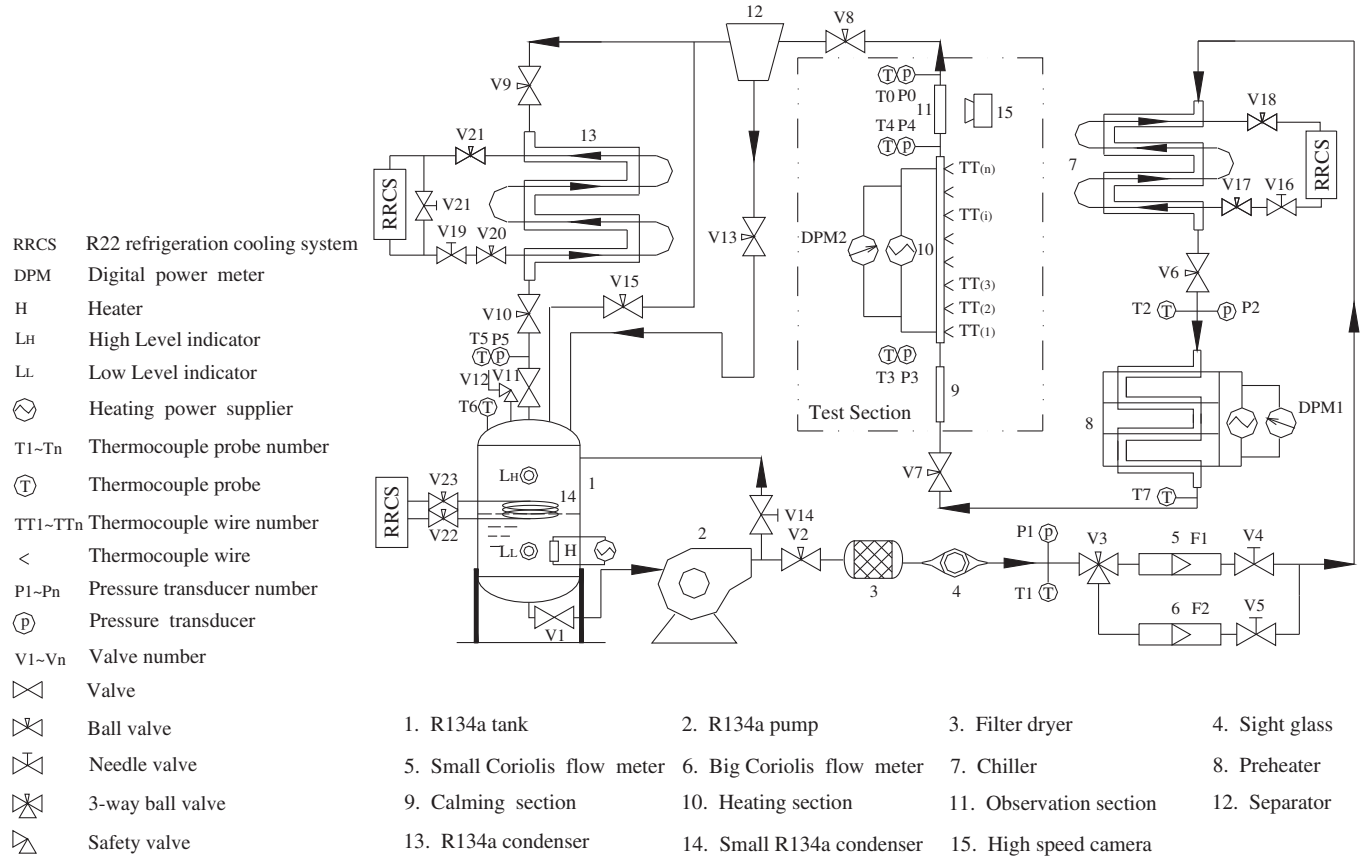

Fig. 3. Schematic diagram of the main R134a plant, Huo et al. [15].

Table 1
The investigated test tubes.

	Welded	Cold drawn		
Inner diameter/wall thickness (mm)	1.16/0.16	1.1/0.25	1.1/0.25	1.1/0.25
Heated length (mm)	150	150	300	450
Number of thermocouples	14	13	14	14
Spacing between thermocouples (mm)	10	10	20	30
Spacing from the lower electrode (mm)	10	15	15	30
Spacing from the upper electrode (mm)	10	15	25	30

connections between the power supply and the test section electrodes. The outer surface temperature was locally measured by fourteen K-type thermocouples with a mean absolute error of ±0.22 K except the shortest cold drawn tube (L = 150 mm) where thirteen thermocouples were used. All thermocouples were attached at equal distances along the test section using an electrically insulating but thermally conducting epoxy. The first and last thermocouples were located away from the electrodes to avoid the effect of heat losses at the electrodes on the measured temperature. The details of the test section are shown schematically in Fig. 4. Fluid temperature and pressure were measured at the test section inlet and outlet using T-type thermocouples with an accuracy of ±0.1 K and pressure transducers with an accuracy of ±0.32%, respectively. The pressure drop was directly measured between the test section inlet and outlet using a differential pressure transducer (Omega PX771A-025DI) with an accuracy of ±0.1%. It is worth mentioning that, there are no flow restrictions at the test section inlet and outlet. A Phantom V4 digital high speed camera with 1000 frame/s and resolution of 512 × 512 pixels was used for flow visualization. The data were monitored through a Labview program at a frequency of 1 Hz using three data loggers: Solatron models SI35951E (two) and SI35351C. All the data were recorded for 90 s after attaining steady state and the sample of the 90 data points was averaged and used in the calculations. Steady state was considered to be achieved when the signals reach their minimum values of oscillations. Fig. 5 depicts one example for the oscillations in the fluid inlet temperature and pressure at 6 bar system pressure and 300 kg/m^2 s mass flux. The figure indicates that, at zero heat flux value, the oscillations in the fluid inlet temperature and pressure were 0.29% and 0.015% of the mean value, respectively. These values increased to 1.13% and 0.77% at the highest heat flux value (97 kW/m^2), which are still very small. Similar stability graphs for the mass flow rate and wall temperature were also obtained. These graphs indicated that the maximum oscillations (at a heat flux value of 97 kW/m^2) in mass flow rate and wall temperature reached 5.5% and 0.63% respectively, which are also very small. This confirms that the experimental data presented in this study correspond to stable boiling.

The local flow boiling heat transfer coefficient $\alpha_{tp}(z)$ was calculated using Eq. (1) and the local vapour quality $x(z)$ was calculated using Eq. (2).

$$\alpha_{tp}(z) = \frac{q''}{T_{wi}(z) - T_{sat}(z)} \tag{1}$$

$$x(z) = \frac{h(z) - h_f(z)}{h_{fg}(z)} \tag{2}$$

where q'' is the heat flux, $T_{wi}(z)$ is the local inner wall temperature, $T_{sat}(z)$ is the local saturation temperature at the local saturation

pressure, $h(z)$ is the local enthalpy, $h_f(z)$ is the local enthalpy of saturated liquid at the local saturation pressure, $h_{fg}(z)$ is the local latent heat at the local saturation pressure and z is the axial distance. The details of calculating each parameter are given in [12,19]. Experimental uncertainties were calculated based on the method given in Coleman and Steele [34] and estimated as a mean absolute value of 6% for the local flow boiling heat transfer coefficient. Single phase validation was conducted for all tubes before starting boiling experiments and the results were presented in [19]. In summary, the validation results indicated that the measured friction factor in all tubes is in a good agreement with the laminar flow theory and Blasius equation [35]. The single phase heat transfer coefficient in the laminar region for all tubes agreed reasonably with the correlation of Shah and London [36] for hydrodynamically developed/thermally developing flow. In the turbulent region, the heat transfer coefficient for all tubes agreed with the Dittus and Boelter equation [37] and with the Petukhov equation [38] except the welded tube in which the measured Nusselt number was higher than the Petukhov equation for Re $\gtrsim$ 5000. The deviation increased with increasing Reynolds number where it ranged from 18% at Re = 5471–107% at Re = 15,504. This could be due to the presence of local anomalies on the surface of this tube as will be discussed later, see also [19], which may create additional local turbulence and thus heat transfer enhancement when the Reynolds number increases.

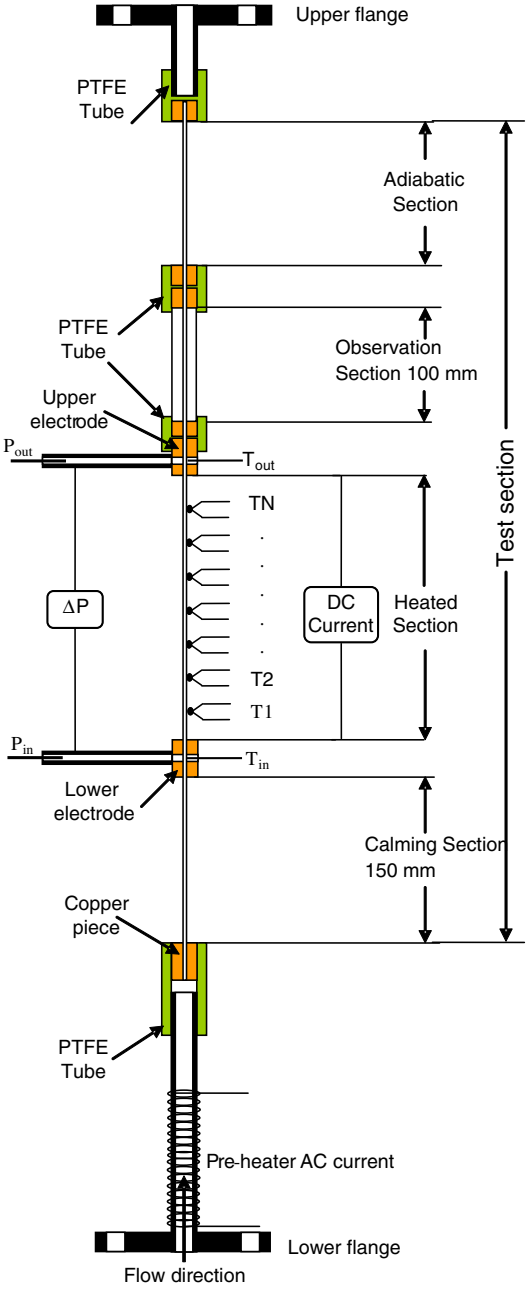

Fig. 4. Schematic drawing of the test section.

3. Sem analysis

As previously mentioned, two stainless steel tubes manufactured by two different processes (welded versus cold drawn) were used to investigate the effect of inner surface characteristics on the local flow boiling heat transfer behaviour. Therefore, a sample of the welded and cold drawn tubes was examined first by the scanning electron microscope (SEM). Each sample was prepared by cutting the tube carefully into two halves using a grinding technique without touching the inner surface as depicted in Fig. 6.

The results of the SEM analysis for the welded tube and the seamless cold drawn tube are shown in Fig. 7. In this figure, picture (a) shows that the surface of the welded tube is very smooth with the presence of some fragments or debris. On the other hand, picture (b) shows that the inner surface characteristics of the seamless cold drawn tube are completely different from those of the welded tube. The surface shows several longitudinal and uniform scratches which may play a significant role in flow boiling heat transfer characteristics compared to the welded tube. Accordingly, it was interesting to reduce the scale of the SEM from 10 μm to 2 μm to see whether these scratches form some type of cavities or not. The result of this examination is depicted in Fig. 8 which shows one cavity (marked by an ellipse in the figure). The difference between the inner surface characteristics of the welded and seamless cold drawn tubes could be attributed to the effect of the manufacturing process. The fabrication of seamless cold drawn tubes starts with hot extrusion process to form the hollow shape of the tube. Since the mandrels used in the hot extrusion process have standard sizes, a cold drawn process is used for further size reduction. Therefore, the longitudinal scratches on the surface of the cold drawn tube may be arising from the tensile stresses resulting from the drawing process. On the other hand, the fabrication of the welded tubes starts with rolling a strip of metal with the required thickness and joining the edges together using advanced welding techniques such as laser welding. Accordingly, if the initial metal strip is smooth, the final inner tube surface will be smooth. This may explain why the inner surface of the welded tube looks very smooth. The fragments or debris observed on the surface may be due to the quality of welding technique, e.g. if the laser beam leaked to the inner surface for any reason, the surface may be damaged locally. After doing the SEM analysis, the surface roughness of the same piece of tube was measured using Taylor Hobson equipment (the piece was adjusted horizontally and the surface was characterized using a contact sensor that traversed 5.1 mm length in the axial direction) and the values were as follows: 1.27 μm for the average roughness of the cold drawn tube compared to 0.52 μm for the welded tube. The peak to valley value was 12.94 μm for the cold drawn tube compared to 4.2 μm for the welded tube. These values indicate how smooth the welded tube surface was.

4. Effect of inner surface characteristics

This section presents and discusses the flow patterns and heat transfer results of the welded and seamless cold drawn tube at

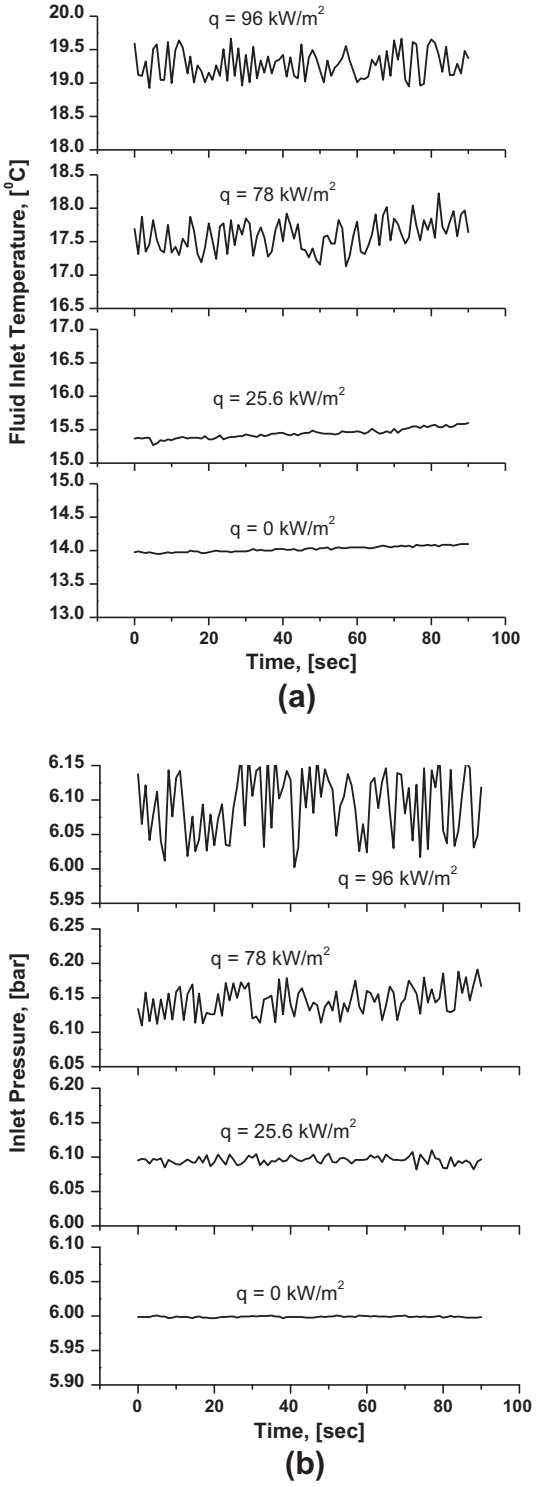

Fig. 5. Steady state oscillations in (a) Fluid inlet temperature and (b) Fluid inlet pressure for $D = 1.1$ mm, $L = 150$ mm at $P = 6$ bar and $G = 300$ kg/m^2 s as a function of heat flux.

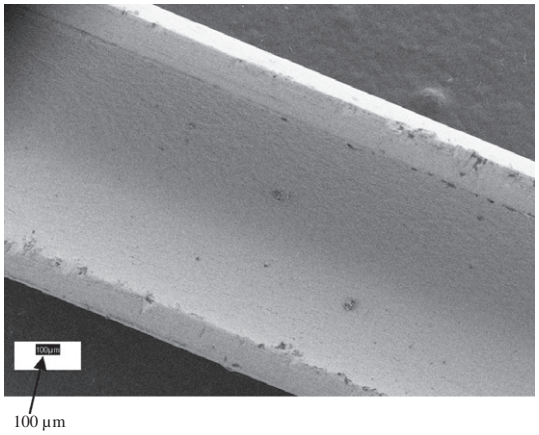

Fig. 6. A sample of the welded tube prepared for the SEM examination by the grinding technique.

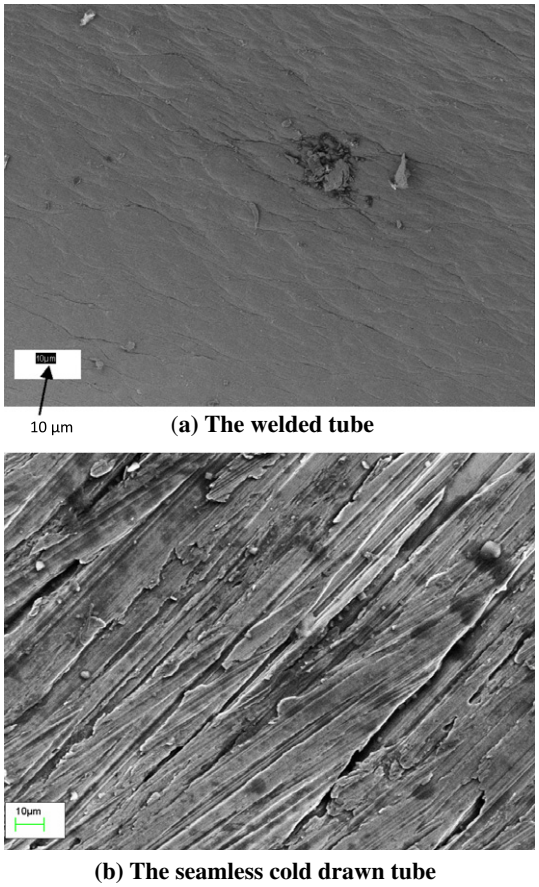

Fig. 7. SEM analysis for the inner surface of the 1.16 mm diameter welded tube and the 1.1 mm diameter seamless cold drawn tube.

8 bar system pressure and 300 kg/m^2 s mass flux. The heat transfer results were presented recently in [19] and were included here so as to provide a complete picture of the effect of the two parameters (surface characteristics and heated length) on the local heat transfer behaviour and to clarify how much they may contribute in explaining the discrepancy in the open literature. The flow patterns and the effect of heat and mass flux on the measured heat transfer coefficient in both tubes are also presented below.

4.1. Flow patterns

Figs. 9 and 10 show the typically observed flow patterns in the seamless cold drawn tube and the welded tube at $G = 300$ kg/m^2 s and $P = 6$ bar. For the seamless cold drawn tube, Fig. 9 shows that the observed flow regimes are bubbly, slug, churn and annular with slug, churn and annular dominating. In slug flow, small

bubbles with a tip-like shape attached to the wall were observed in the liquid slug between consecutive bubbles as seen in the third picture from the left and also tiny bubbles were observed trapped in the liquid film as seen in the fourth picture from the left in Fig. 9. As the heat flux increased, the slug length increased and the elongated slugs merged and resulted in a wide churning zone with the appearance of liquid slugs in some pictures, see the third picture from the right. With further increase in heat flux, the liquid slugs disappeared and churn flow with a highly chaotic liquid/vapour interface developed. At $x = 0.44$, the features of annular flow appeared with a rough liquid/vapour interface as seen in the last picture in Fig. 9. Also, the picture shows that there are liquid droplets entrained into the vapour core due to the breakup of the liquid film.

Fig. 10 indicates that the observed flow regimes in the welded tube are slug, churn and annular flows. It is worth mentioning that bubbles of the shape of the first picture from the left were also referred as confined bubbles by, for example [32]. It is obvious that the difference between the flow patterns in the two tubes appears only at low heat flux (low exit quality). In the welded tube, bubbly flow was not observed whereas bubbly flow was observed in a few pictures in the cold drawn tube. Once boiling started, a train of short vapour slugs with almost uniform length appeared in the welded tube as seen in Fig. 10 at $x = 0.022$. Moreover, no tiny bubbles were observed in the liquid slugs between the consecutive bubbles. The absence of this kind of bubbles in the welded tube at the lowest heat flux could be attributed to the effect of the tube inner surface characteristics. As previously discussed, the surface of the welded tube is very smooth with the existence of some local anomalies or debris on the surface. These anomalies are defects resulting from the manufacturing process and they are not uniformly distributed along the length of the tube. In addition to that, the geometrical shape of the debris is not uniform and thus they may work as a nucleation cavity or may not. As a result, nucleation in the welded tube may commence only at some limited locations, which could be far away from the exit of the heated section (inlet of visualization section), i.e. in the first half of the tube. Accordingly, the nucleating bubble may then have a good chance to grow and form the well-ordered bubble train slug flow inside the heated section before it reaches to the visualization section especially if they have formed near the entry of the heated test section. The resulting vapour slug may also reduce nucleation further away from the entry section of the tube. The appearance of the well-ordered bubble train slug flow in the visualization section may confirm that only very few sites are active and stable. On the contrary, the inner surface of the cold drawn tube is uniformly scratched along the tube length. Therefore, more nucleation sites may exist

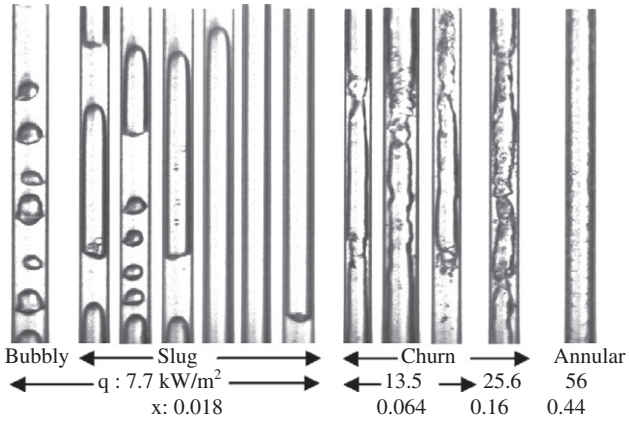

Fig. 9. Flow patterns observed at the exit of the 1.1 mm diameter seamless cold drawn tube, $L = 150$ mm at $G = 300$ kg/m^2 s, $P = 6$ bar as a function of exit quality and heat flux in kW/m^2.

along the length of the tube and there is a possibility for nucleation to occur at locations all along the heated section, i.e. bubbly flow and the tiny bubbles with a tip-like shape appeared with the seamless cold drawn tube. As the heat flux increased ($x = 0.051$), some of the well-ordered slug flow converted into elongated slugs which appeared in a considerable number of pictures compared to the seamless cold drawn tube. With further increase in heat flux, the features of the flow regimes in the welded and the seamless cold drawn tube were almost similar until the development of annular flow. Generally, the most frequently observed flow patterns in both tubes are: slug, churn and annular.

4.2. Effect of heat flux

Mahmoud et al. [19] presented the heat transfer results of the welded and cold drawn tubes as a function of heat flux, vapour quality and axial distance at $P = 8$ bar and $G = 300$ kg/m^2 s. Fig. 11 depicts the heat flux effect for the welded tube as a function of the local vapour quality. It is obvious from the figure that, the trend of the local heat transfer coefficient versus local vapour quality is peculiar and was not observed before in the experiments of this group or to the best of our knowledge, the work of other researchers. Additionally, the effect of heat flux is not clear and seems difficult to be deduced from this plot. The figure indicates that, for most heat fluxes after the entry region, the heat transfer coefficient decreases rapidly to a

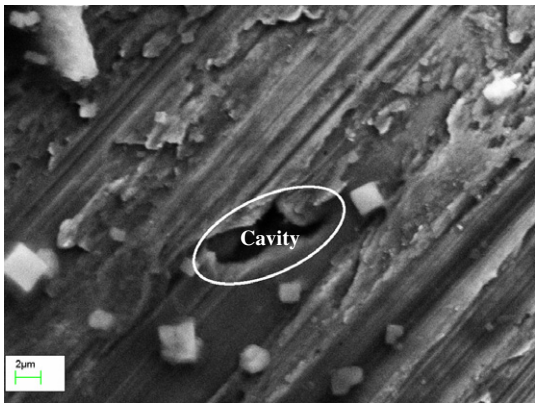

Fig. 8. SEM analysis of the inner surface analyses for the inner surface of the seamless cold drawn tube of 1.1 mm diameter that shows one cavity.

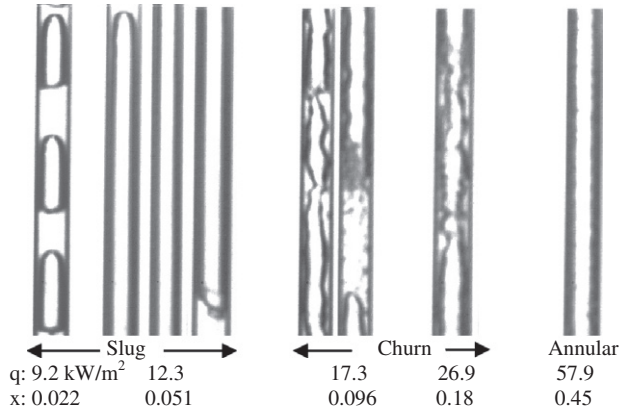

Fig. 10. Flow patterns observed at the exit of the 1.16 mm diameter welded tube, $L = 150$ mm at $G = 300$ kg/m^2 s, $P = 6$ bar as a function of exit quality and heat flux in kW/m^2.

minimum value after which it increases rapidly with quality before it decreases again at the last thermocouple location. In the entry region, the heat transfer coefficient jumped from its single phase value to a very high value at $x \approx 0$ due to the onset of nucleate boiling. The axial distance plot, Fig. 12, demonstrated some minimal effect of heat flux but for some regions all the lines approximately merged ($z = 0.04$–0.06 m and $z > 0.12$ m). On the contrary, a clear heat flux effect was detected in the cold drawn tube as seen in Figs. 13 and 14. The heat transfer coefficient increased with increasing heat flux with small dependency on local vapour quality and axial distance.

The boiling curves plotted for the welded and cold drawn tubes at three axial locations (representing the entry region, the middle section and the exit region) from [19] and are depicted in Fig. 15. The figure again indicates that there is a difference between the welded and the cold drawn tube. The welded tube required a very high wall superheat to trigger fully developed nucleate boiling at all locations (a value of about 14.2–17.4 K was required). On the contrary, fully developed nucleate boiling commenced in the cold drawn tube at a lower wall superheat value of about 3.2–3.7 K at all locations except the entry region. In the entry region, the stability of the nucleation sites may be influenced by the small variations in the inlet sub-cooling. It was difficult to keep the inlet sub-cooling constant at exactly 5 K but it was varying within about ±1 K. This may also be clear from the shape of the boiling curve in the entry region for both tubes (Fig. 15a), which is completely different compared to the middle and exit locations. Normally, after the onset of nucleate boiling, the wall superheat increases slightly with increasing heat flux until dryout occurs as is the case in Fig. 15b and c. By contrast, Fig. 15a shows that, after the onset of nucleate boiling, the wall superheat continued decreasing with increasing heat flux up to $q = 41$ kW/m^2 for the welded tube and up to 25 kW/m^2 for the cold drawn tube. At the middle location, both tubes demonstrated similar behaviour after the onset of the fully developed nucleate boiling.

The above results demonstrate that there is a clear difference in heat transfer behaviour between the cold drawn and welded tube. Since the two investigated tubes were similar in dimension, design and instrumentation, Mahmoud et al. [19] attributed the difference in heat transfer behaviour to the difference in the inner surface characteristics resulting from the manufacturing process. The manufacturing process of the microtubes was not taken into consideration in the past studies by any research group. As presented previously in Fig. 7, the inner surface of the welded tube was very smooth with the existence of a number of anomalies on the surface. These anomalies may work as active nucleation sites or may not, depending on the size and shape of each anomaly, which seems from Fig. 7a to have an irregular shape. The smoothness of the surface may explain the high wall superheat required at the onset of nucleate boiling at all axial locations as presented in Fig. 15. Also, the very limited number of nucleation sites in the smooth surface, which seem not uniformly distributed along the tube, may explain the non uniformity of the local heat transfer coefficient along the tube and the small heat flux effect. The heat transfer results of the welded tube (smooth surface with few nucleation sites) may be used to give a rough picture for the trend of the local heat transfer coefficient that would result if the nucleation process was suppressed. By contrast, Fig. 7b depicts a completely different texture for the inner surface of the seamless cold drawn tube. The random scratches on the surface of this tube, which seem uniformly distributed along the tube, seem to form the type of cavities that are required for the nucleation process. Accordingly, there is a possibility for nucleation to occur all along the tube which may explain the clear heat flux effect.

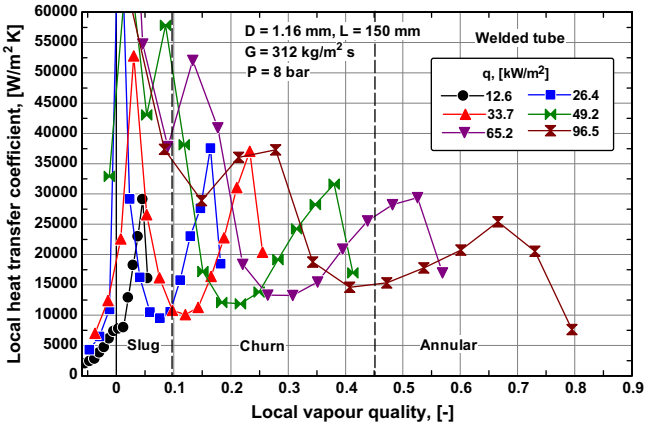

Fig. 11. The effect of heat flux for the welded tube as a function of vapour quality at $P = 8$ bar and $G = 300$ kg/m^2 s [19].

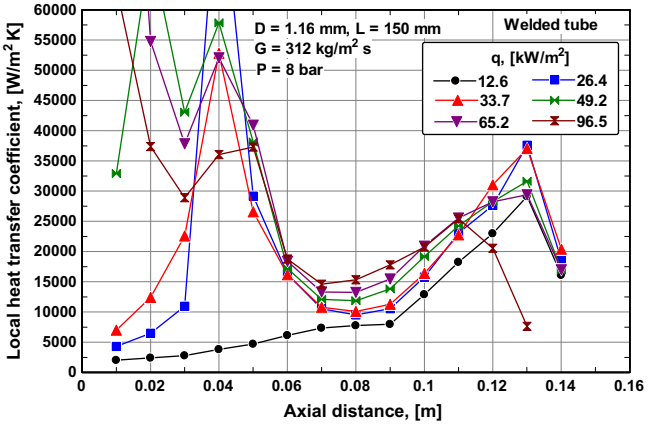

Fig. 12. The effect of heat flux for the welded tube as a function of axial distance at $P = 8$ bar and $G = 300$ kg/m^2 s [19].

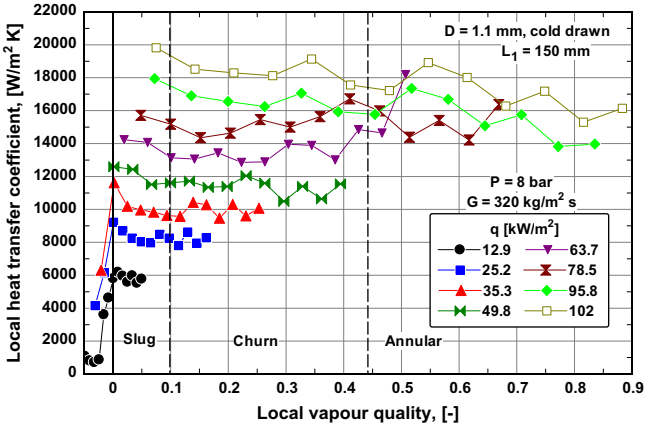

Fig. 13. The effect of heat flux for the seamless cold drawn tube as a function of vapour quality at $P = 8$ bar and $G = 300$ kg/m^2 s [19].

4.3. Effect of mass flux

Fig. 16 illustrates the effect of mass flux on the local heat transfer coefficient at $q = 41$ kW/m^2 for the welded tube and Fig. 17 presents the mass flux effect for the seamless cold drawn tube at the same condition. Examination of Fig. 16 indicates again, that the

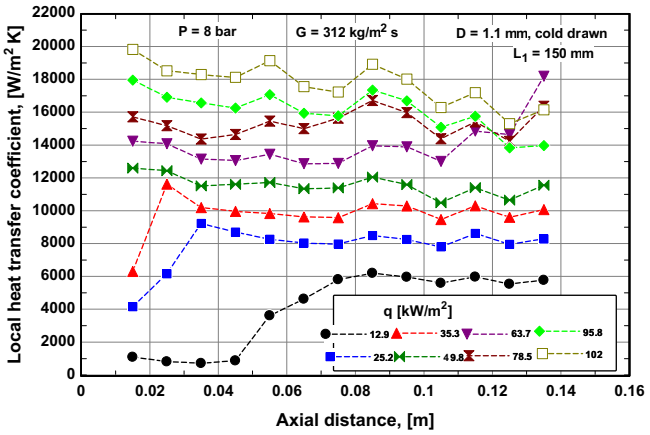

Fig. 14. The effect of heat flux for the seamless cold drawn tube as a function of axial distance at $P = 8$ bar and $G = 300$ kg/m^2 s [19].

mass flux effect seems complex and difficult to deduce from the vapour quality plot (Fig. 16a), while the axial distance plot (Fig. 16b) shows a rather insignificant effect. On the contrary, both the quality and axial distance plots of the seamless cold drawn tube (Fig. 17) do not show any mass flux effect and all the lines merge into a single line. Conventionally, nucleate boiling dominates when the heat transfer coefficient increases with heat flux but does not depend on quality and mass flux whilst convective boiling dominates when the coefficient increases with quality and mass flux but does not depend on heat flux. Applying and solely based on these criteria, it can be concluded that nucleate boiling may be the dominant heat transfer mechanism at intermediate quality ranges in the cold drawn tube. The mechanism in the welded tube is unclear and very difficult to infer.

5. Effect of heated length

This section presents and discusses the heat transfer results for a seamless cold drawn tube of 1.1 mm inner diameter and three different heated lengths (150, 300, 450 mm). The effect of heat flux, mass flux and system pressure are discussed below. The flow patterns observed in the shortest and longest tubes are presented first.

5.1. Flow patterns

Fig. 18 depicts the flow patterns of the longest tube, ($L = 450$ mm) at 6 bar system pressure and 300 kg/m^2 s mass flux. This should be compared with Fig. 9, which depicts the typically observed patterns for the shortest length ($L = 150$ mm). Figs. 9 and 18 demonstrate that, three regimes dominate for all tubes namely slug, churn and annular flow regimes. It is obvious that, annular flow appears early at lower vapour quality for the longer heated section ($x = 0.44$ for $L = 150$ mm and $x = 0.25$ for $L = 450$ mm). It is important to note that, the heated length will significantly affect the flow patterns if the comparison was conducted at the same heat flux. For example, for $q = 7.7$ kW/m^2 the flow pattern is slug in the shortest tube whilst it is churn in the longer tube at $q = 7.6$ kW/m^2. The comparison at a fixed heat flux means that the exit vapour quality of the longest tube will be much greater than the exit vapour quality of the shortest one. Consequently, the flow patterns observed at the exit of each tube are expected to be different. Further work is needed to assess fully the effect of the heated length on the flow patterns.

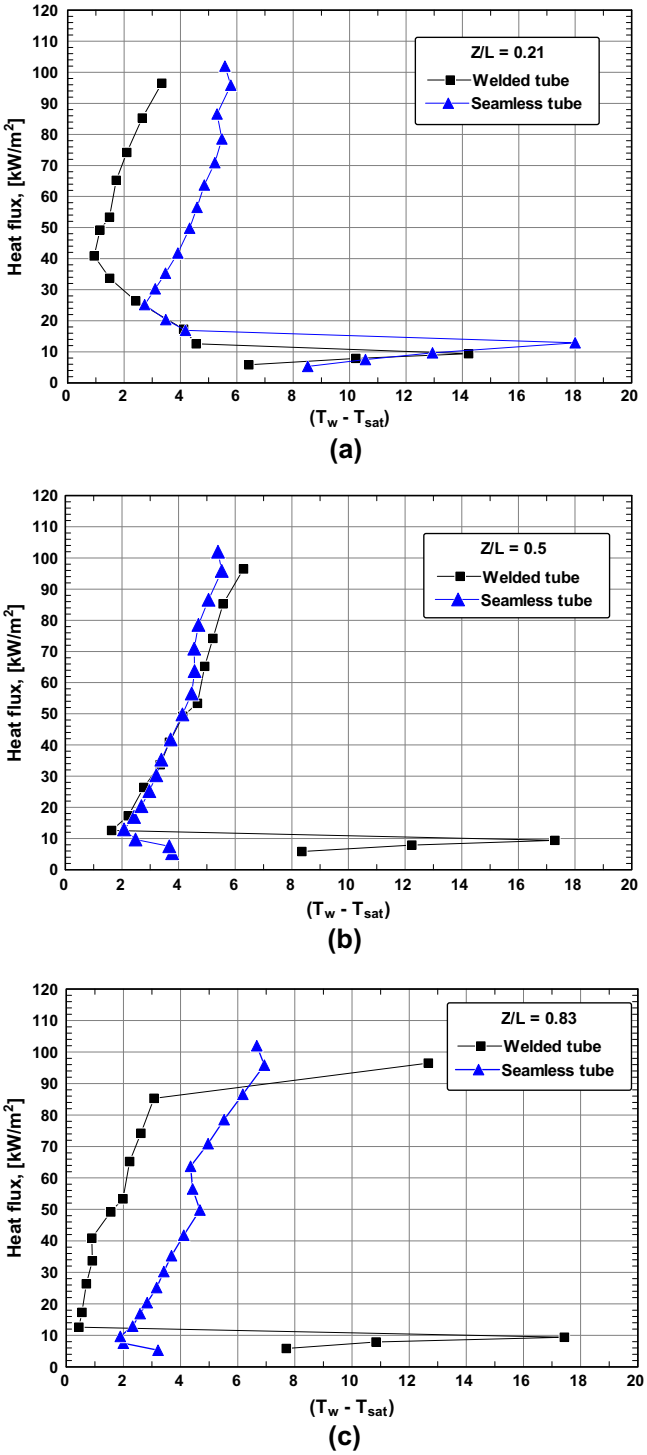

Fig. 15. The boiling curves plotted through increasing heat flux at the axial locations for the welded and seamless tubes: (a) at location near from the entry region, (b) at middle location, (c) at location near exit [19].

5.2. Effect of heat flux

Fig. 19 depicts the effect of heat flux on the local heat transfer coefficient for the three heated lengths at $G = 300$ kg/m^2 s and $P = 6$ bar as a function of vapour quality. The experimental flow patterns transition boundaries are also shown on the figures. The trend of the heat transfer coefficient in Fig. 19a is similar to the one presented and discussed previously in Fig. 13 at 8 bar system pressure. It is obvious from Fig. 19a that, the heat transfer

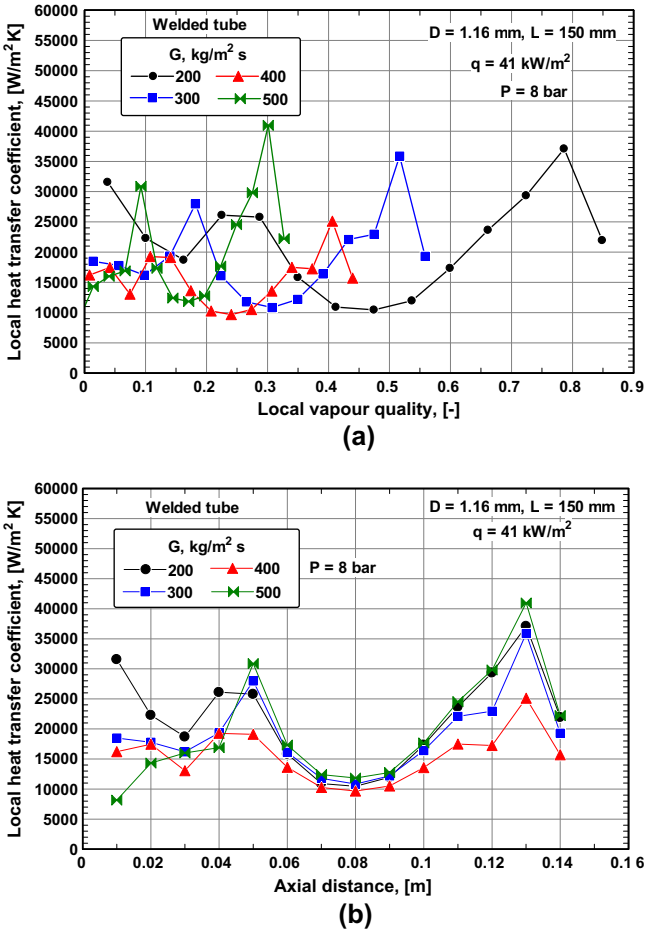

Fig. 16. The mass flux effect for the welded tube at $q \approx 41$ kW/m^2 (a) quality plot, (b) axial distance plot, [19].

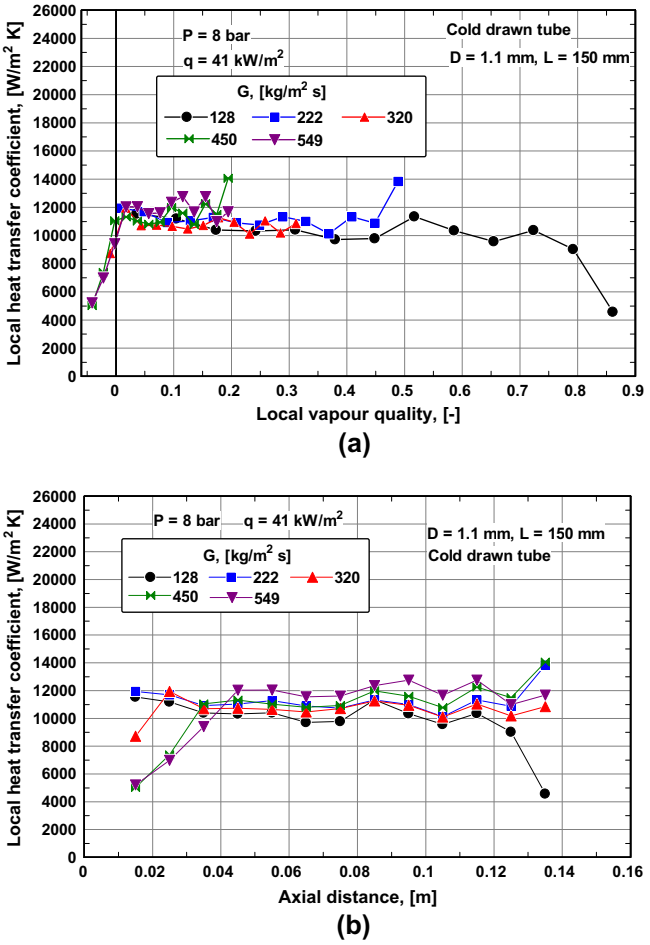

Fig. 17. The mass flux effect for the seamless cold drawn tube at $q \approx 41$ kW/m^2 (a) quality plot, (b) axial distance plot [19].

coefficient increases with heat flux with little dependence on local vapour quality. At low heat fluxes where a considerable length of the tube is under single phase conditions, the heat transfer coefficient jumps at vapour quality values close to zero then it drops before it remains approximately constant with quality. Also, it is obvious that, the heat transfer coefficient tends to increase with quality at locations near the tube exit, which is clear at heat flux values of 64.1 and 78.6 kW/m^2. For $q \geqslant 95.7$ kW/m^2, the effect of heat flux appeared to be insignificant and dryout occurred at $x \approx 0.52$. Fig. 19b demonstrates for $L = 300$ mm that the trend of the local heat transfer coefficient changes with heat flux. At low heat flux values ($q = 7.5$ and 13.7 kW/m^2), the trend was similar to N-shape starting from the single phase region. The coefficient jumped from its single phase value and peaked at local quality values near to zero then suddenly dropped to a minimum value before it rapidly increases with vapour quality. At intermediate heat flux values, ($q = 25.4$–35.4 kW/m^2), the minima that appeared at lower heat fluxes have diminished and the trend changed. At these conditions, after the heat transfer coefficient increased from its single phase value to its maximum value, it showed little dependence on vapour quality up to $x = 0.25$. After this quality value, the heat transfer coefficient increased with vapour quality and the curves collapsed into one single line. Another change in the trend was observed at high heat flux values ($q = 41$–55.8 kW/m^2). The heat transfer coefficient decreased from its maximum value at $x \approx 0.01$ up to a vapour quality value of about $x = 0.13$ then it remained approximately constant with quality until dryout occurred at $x \approx 0.6$. Additionally, it is obvious from the figure that the heat transfer coefficient increases with heat flux up to $x \approx 0.3$ especially at low to intermediate heat flux values. At the three highest heat fluxes, the heat flux effect was not so significant. Fig. 19c depicts the results for the longest tube and demonstrates that, for the lowest heat flux ($q = 5$ kW/m^2), the heat transfer coefficient remained very small up to thermocouple location no. 12 ($Z/L = 0.8$) at which boiling commenced and the heat transfer coefficient jumped from about 600 W/m^2 K to 4600 W/m^2 K. For intermediate heat flux

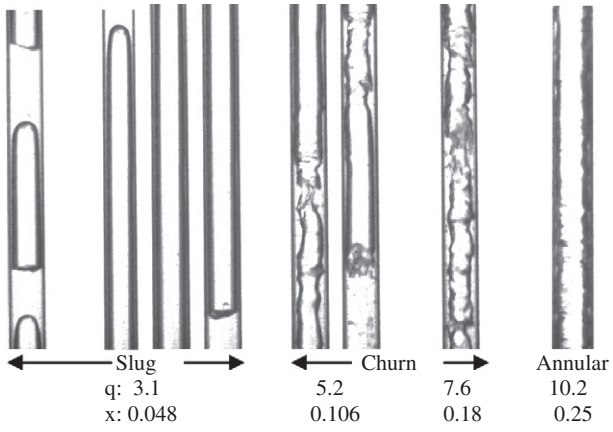

Fig. 18. Flow patterns observed at the exit of the 1.1 mm diameter seamless cold drawn tube, $L = 450$ mm at $G = 300$ kg/m^2 s and $P = 6$ bar.

values (q = 10–25.3 kW/m^2), the heat transfer coefficient drops from its maximum value at vapour quality close to zero then it remains approximately constant with vapour quality up to thermocouple location no. 6 (Z/L = 0.4). After this location, the heat transfer coefficient slightly drops up to location no. 7 (Z/L = 0.47) then it increases constantly with vapour quality. For the two highest heat fluxes (q = 30–35.4 kW/m^2), the trend is similar to the intermediate heat flux up to local vapour quality of 0.3. At vapour qualities greater than this value, the two lines merged together with little dependency on vapour quality and heat flux up to x = 0.82, after which dryout occurred. The figure indicates also that there is a clear heat flux effect for vapour qualities less than about 0.3.

Fig. 20 depicts the axial distance plots for the three heated lengths. Fig. 20a shows that, after boiling incipience, the heat transfer coefficient increases with heat flux with little dependence on axial distance. Some increase with axial distance is observed near to tube exit especially for q = 64.1 and 78.6 kW/m^2. Fig. 20b indicates that for all heat fluxes, the heat transfer coefficient decreases immediately after boiling incipience. After an axial distance of about Z/L = 0.52 (z = 156 mm), the heat transfer

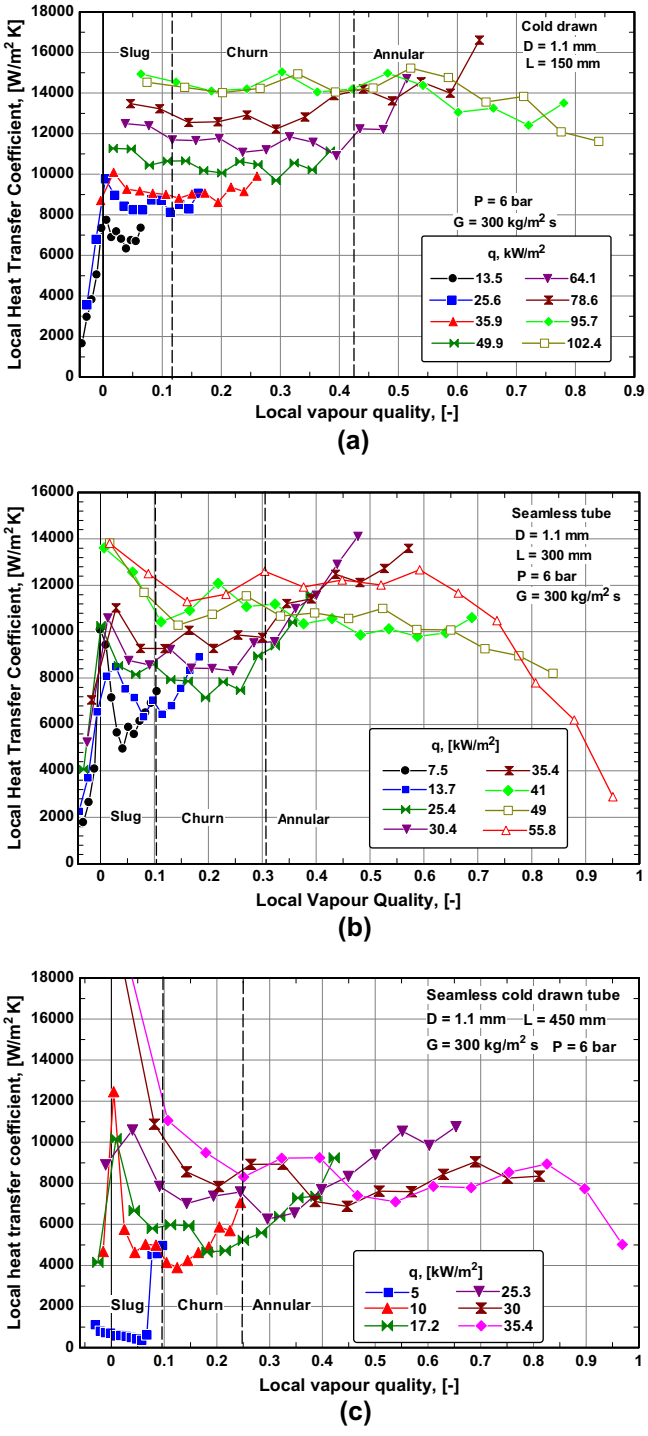

Fig. 19. The effect of heat flux on the local heat transfer coefficient as a function of local vapour quality at P = 6 bar, G = 300 kg/m^2 s, D = 1.1 mm.

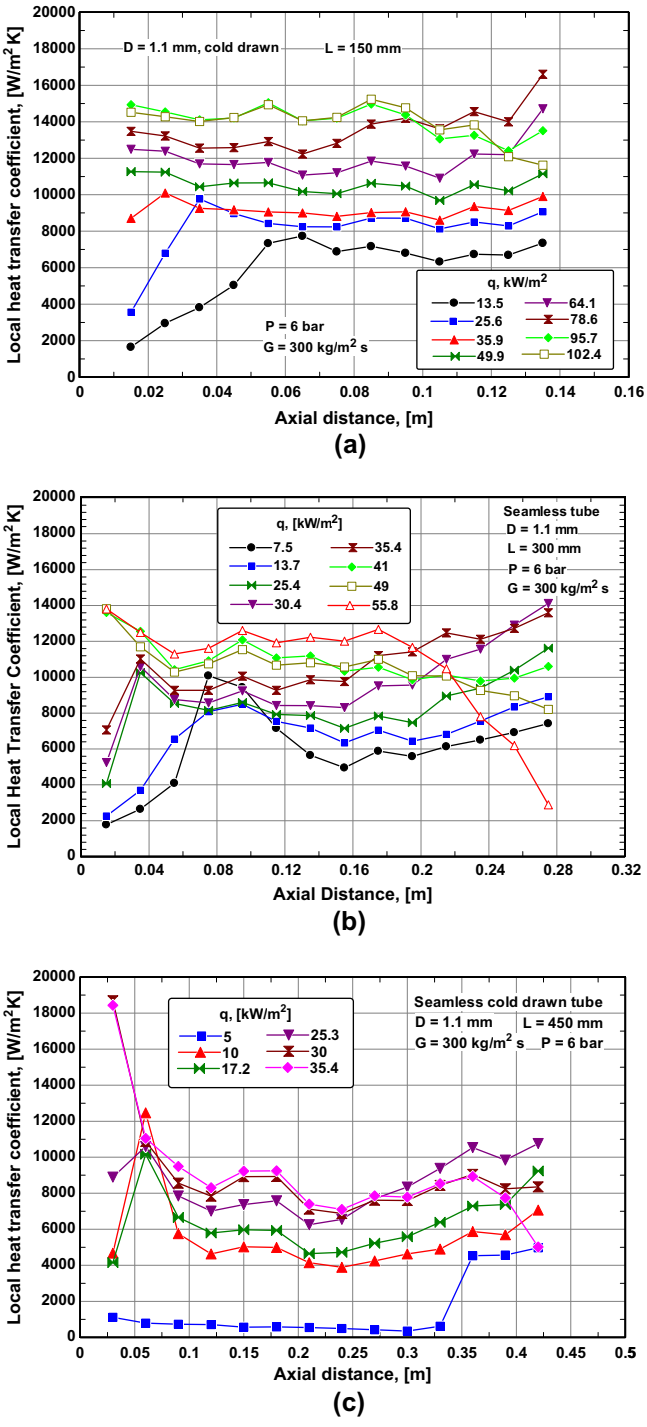

Fig. 20. The effect of heat flux on the local heat transfer coefficient as a function of axial distance at P = 6 bar, G = 300 kg/m^2 s, D = 1.1 mm.

coefficient increases with distance and heat flux up to $q = 35.4$ kW/m^2. Also, it is obvious that, the effect of heat flux is small in the first half of the tube compared to the second half towards the exit. Fig. 21c demonstrates that there is an unclear heat flux effect on the heat transfer coefficient at locations $Z/L < 0.1$, which are near from the location of boiling incipience. After this location, the lines were separated indicating a clear heat flux effect with little dependence on axial distance for $Z/L = 0.2$–0.47. After $Z/L = 0.47$, the heat transfer coefficient increased rapidly with axial distance for heat fluxes up to 25.3 kW/m^2 whilst the increasing rate decreased with the two highest heat fluxes before dryout.

5.3. Effect of mass flux

Figs. 21 and 22 illustrate the effect of mass flux on the local heat transfer coefficient for the three heated lengths at 6 bar system pressure as a function of quality and axial distance, respectively. Fig. 21a shows that the effect of mass flux on the local heat transfer coefficient is not significant in the shortest tube ($L = 150$ mm). On the other hand, Fig. 21b and c demonstrates that although there is no mass flux effect up to quality values of 0.2–0.25, after this value the mass flux effect is clear, i.e. the heat transfer coefficient increases with increasing mass flux. On the contrary, however the plots with axial distance in Fig. 22 do not show a clear mass flux effect for any of the three tubes.

5.4. Effect of system pressure

Fig. 23 presents the effect of system pressure on the local heat transfer coefficient for the three heated lengths. Fig. 23a and b shows that the heat transfer coefficient increases with increasing system pressure for $L = 150$ and 300 mm. On the other hand, Fig. 23c shows for $L = 450$ mm that the heat transfer coefficient increases with system pressure up to $x = 0.3$ after which the effect becomes insignificant. The increase of the heat transfer coefficient with increasing system pressure arises from the effect of pressure on surface tension. As the pressure increases from 6 to 10 bar, the surface tension of R134a decreases by about 30%. The reduction in surface tension value results in a reduction in the bubble departure diameter and thus increases the contribution of nucleate boiling. In a recent paper, Yuan et al. [39] demonstrated that bubble size and growth rates decreased as the system pressure increased. As seen in Fig. 23c, this effect is clear at lower quality values where nucleate boiling maybe more dominant. Fig. 23b shows some local peaks in the heat transfer coefficients at thermocouple locations no. 2 and no. 5. It is interesting to note that the magnitude of the peak at these locations increases with increasing system pressure. In other words, these locations seem to be representing nucleation sites and the peak value increases with pressure due to the increase in the bubble generation frequency when the pressure increases.

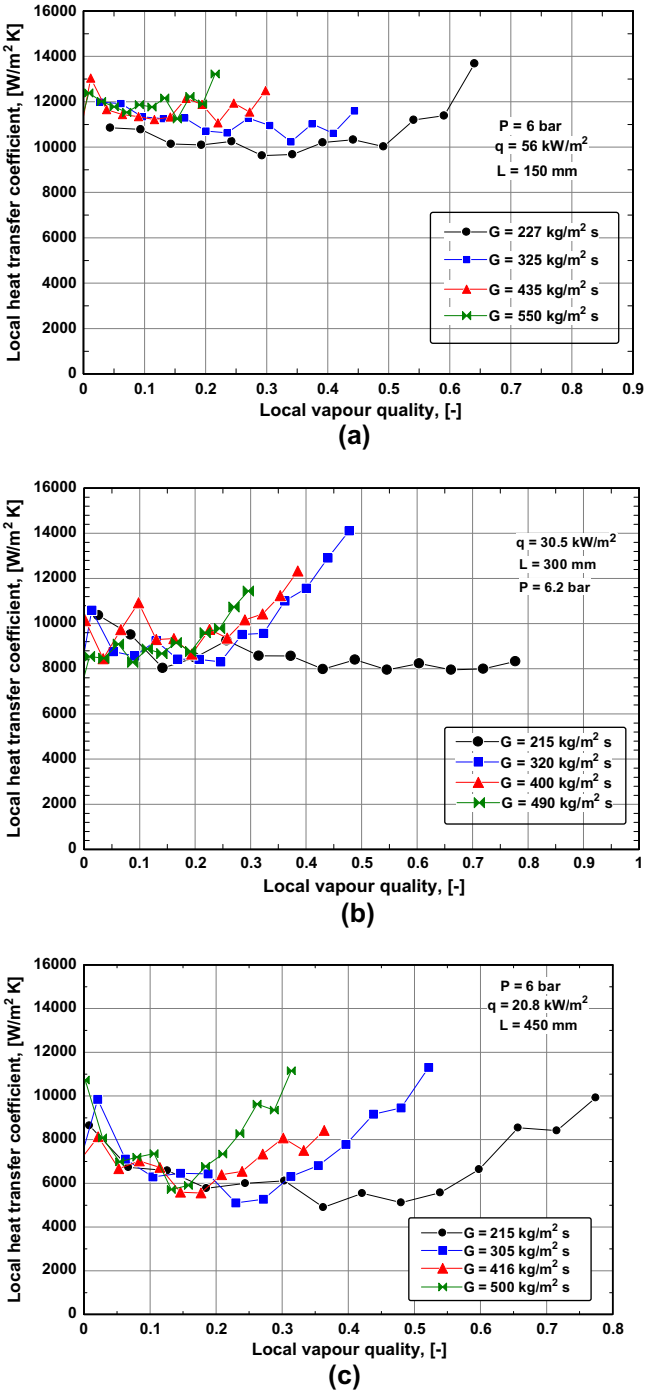

Fig. 21. The mass flux effect at $P = 6$ bar for the three heated lengths as a function of local vapour quality.

5.5. Discussion

The above figures indicate that the heated length influences the behaviour and magnitude of the heat transfer coefficient. All figures agreed on the fact that, the heat transfer coefficient decreases with increasing vapour quality immediately after boiling incipience in the very small quality region. The magnitude of the drop of the heat transfer coefficient from its maximum value at quality close to zero increased with increasing heated length. For $L = 150$ mm, the heat transfer coefficient dropped by 11.6% at $q = 13.5$ kW/m^2 whilst for $L = 300$ mm and $L = 450$ mm it dropped by 50.8% and 59.6%, respectively for $q = 7.5$ kW/m^2 and $q = 10$ kW/m^2, respectively. Lin et al. [40] obtained similar features during the flow boiling of R141b in a 1 mm diameter tube with a 500 mm heated length. They attributed the drop in the heat transfer coefficient after boiling incipience to the inappropriate assumption of linear variation of pressure drop along the tube. They have supported their point using the model of Cornwell and Kew [41] according to which a significant part of the pressure drop occurs at boiling incipience due to the bubble confinement associated with high local pressure fluctuations. The fluctuations in the local pressure during flow boiling in narrow channels were experimentally measured by Aligoodarz et al. [42] and Yan and Kenning [43]. It was found that, the fluctuations in the local pressure attained values that are equivalent to about 2 K fluctuations in the wall superheat. Based on that, Lin et al. [40] believed that the local sat-

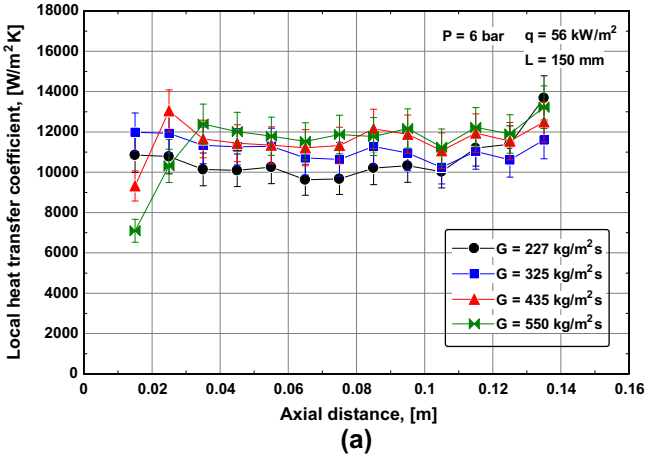

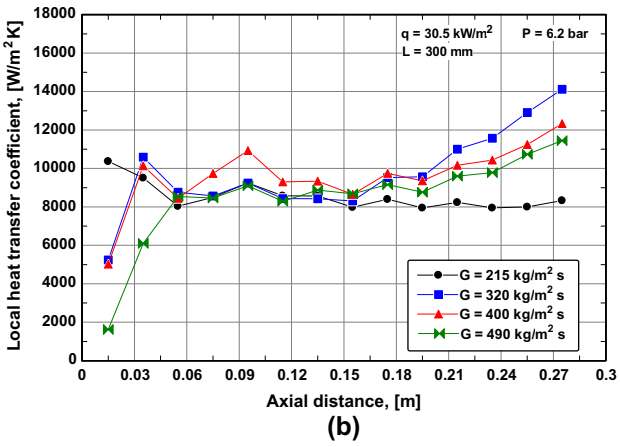

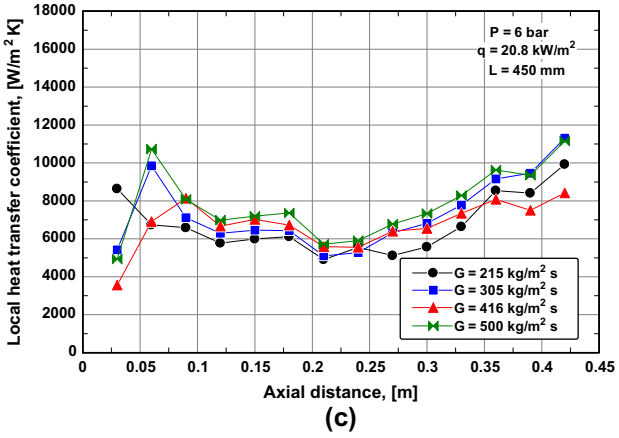

Fig. 22. The mass flux effect at $P = 6$ bar for the three heated lengths as a function of the axial distance.

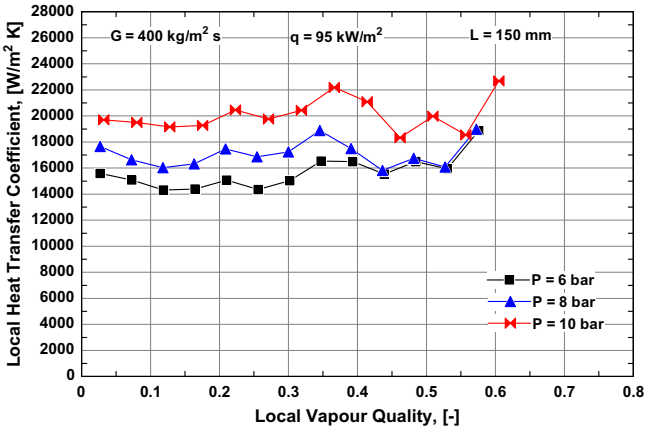

(a) L = 150 mm

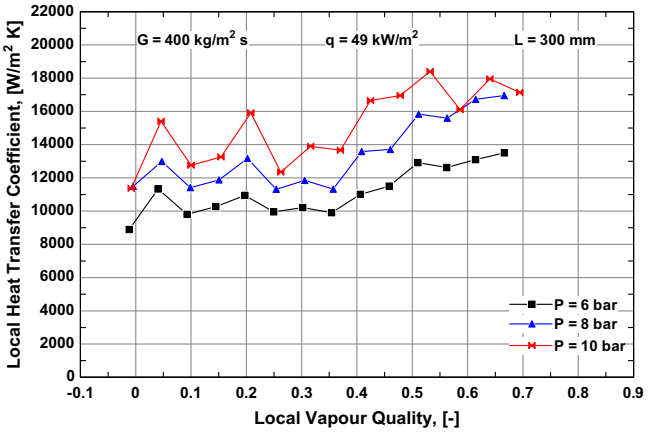

(b) L = 300 mm

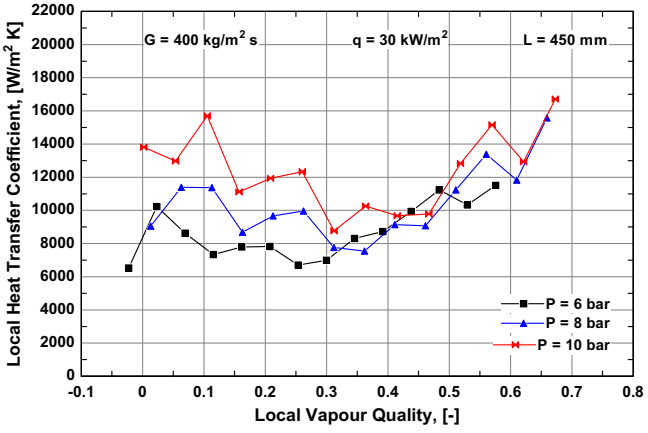

(c) L = 450 mm

Fig. 23. Effect of system pressure on the heat transfer coefficient for the three heated lengths at $G = 400$ kg/m^2 s.

uration temperature and pressure in the region of boiling incipience may be lower than the one estimated based on the linear assumption. The behaviour of the heat transfer coefficient at boiling incipience in the current study may be explained in a similar way. Since the measured pressure drop in the shortest tube is the lowest compared to the other longer lengths, the variation in the local saturation temperature at boiling incipience may be small as well. Additionally, the heat flux required to attain the same exit quality is higher for the shortest tube – the thing that may activate more nucleation sites. Accordingly, the magnitudes of the heat transfer coefficient in the shortest tube after boiling incipience are approximately close to the peak values. Also, Figs. 19 and 20 indicate that the heat flux effect was very clear in the shortest tube ($L = 150$ mm) where separate lines were observed with little dependence on local vapour quality and axial distance over the tube length. Nevertheless, Fig. 19a demonstrates that there was a tendency for the trend to change at $q = 64.1$ kW/m^2. As the heated length was increased, the change of the trend of the heat transfer coefficient versus vapour quality has become more obvious as seen in Fig. 19b and c. The heat transfer coefficient increased with increasing vapour quality over a considerable length of the tube which does not occur in the shortest tube. It is clear from Fig. 19b and c that the heat transfer coefficient increased with vapour quality even at the lowest heat fluxes where the flow pattern

was slug and churn. Possible reasons could be the increase in pressure drop with the increase of the heated length which influences the local saturation temperature. However, the saturation temperature decreased by 0.2%, 0.48% and 1.2% for $L = 150$, 300 and 450 mm respectively which seems to be small to cause this effect. Another possible reason could be the value of heat flux corresponding to the same exit quality where for $x \approx 0.9$ the heat flux was 102.4, 55.8 and 35.4 kW/m^2 for $L = 150$, 300 and 450 mm, respectively. The very high values of heat fluxes in the shortest tube may be sufficient to activate more nucleation sites over a considerable length of the tube. This is clear from Fig. 24 that depicts the effect of the heated length on the magnitudes of the heat transfer coefficient. When the comparison is conducted at the same exit quality (Fig. 24a), the heat transfer coefficient in the shortest tube was the highest. On the other hand, when the comparison is conducted at the same heat flux, the magnitudes were approximately similar in the low quality region. Thus, the low heat flux values in the longer tubes may be sufficient only to activate few numbers of nucleation sites. It is clear from Figs. 19 and 20 that after a certain heat flux value ($q > 35.4$ kW/m^2 for $L = 300$ mm and $q = 25.3$ kW/m^2 for $L = 450$ mm), the increasing trend with vapour quality disappears and the heat transfer coefficient remains approximately unchanged with quality even at very high vapour qualities. This change in trend may be attributed to the features of annular flow observed in the 1.1 mm diameter tube. The pictures demonstrated that there is some liquid entrainment to the vapour core. In this case, the heat transfer coefficient can increase or remain constant depending on the rate of liquid droplet deposition and/or entrainment. If the two rates are approximately equal, the heat transfer coefficient is expected to increase with local quality. On the other hand, if the deposition rate is higher than the entrainment rate the film thickness may build up and the heat transfer coefficient is expected to decrease with quality or remain approximately constant. It appears from Figs. 19 and 21 that, nucleate boiling dominates in the shortest tube even at reasonably high vapour quality. In the longer tubes, nucleate boiling seems to dominate only in the low quality region whereas convective boiling seems to dominate in the intermediate to high quality region. As mentioned above, the dominance of nucleate boiling in the shortest tube may be attributed to the operation at much higher heat fluxes (wall superheat) compared to the longer tubes. It is interesting to note that, when Fig. 24b was re-plotted versus Z/L, where Z is the axial distance and L is the heated length, the effect of the heated length on the magnitude of the heat transfer coefficient was found to be insignificant all along the tube. However, for design purpose, evaporators with short length may be preferable compared to long ones. This may be due to the lower pressure drop per unit heating rate. In Fig. 25, the heating rate for the shortest tube is 12.96 W and the measured pressure drop value is 0.0185 bar, which gives a relative value of 1.43×10^{-3} bar/W. For the longest tube, the heating rate is 38.9 W and the measured pressure drop value is 0.106 bar or 2.74×10^{-3} bar/W, which is 1.9 times higher than that in the shortest tube. Another possible reason for preferring short evaporators could be the uniform heat transfer coefficient along the evaporator, which is obvious from Figs. 19a and 20a where the coefficient was approximately constant with quality and axial distance, respectively. Having almost uniform heat transfer coefficient along the evaporator may simplify the design calculations.

6. Conclusions

The flow boiling characteristics of R134a in 1.1 mm diameter tubes were investigated experimentally in the current study at different experimental conditions. The effect of the heated length and surface finish on the local behaviour of the heat transfer coefficient was investigated. The important conclusions that can be drawn from the current study are summarized as follows:

1. The manufacturing process influences significantly the inner surface of the microtubes. This was confirmed by the SEM analysis that demonstrated that the structure of the inner surface of the welded tube was completely different compared to that of the seamless cold drawn tube. It was also confirmed by the different behaviour of the local heat transfer coefficient in the two tubes.
2. Assessing the inner surface of the manufactured stainless steel microtubes by single phase flow only may not be enough for comparisons of microevaporators. In addition to single phase flow, the inner surface characteristics should be taken into consideration, i.e. at least clearly stated in the reports.
3. The flow boiling characteristics in the welded tube were completely different compared to those in the seamless cold drawn tube. Based on the premise that nucleate boiling dominates when the heat transfer coefficient is independent of quality and mass flux and increases with heat flux one can infer that the heat transfer process in the seamless tube was dominated by the nucleate boiling mechanism before dryout while the welded tube does not show a clear dominant mechanism.
4. The most frequently observed flow patterns were slug, churn and annular flow. Increasing the heated length resulted in a decrease in the vapour quality at which a transition into annular flow occurs. The inner surface characteristics seem to

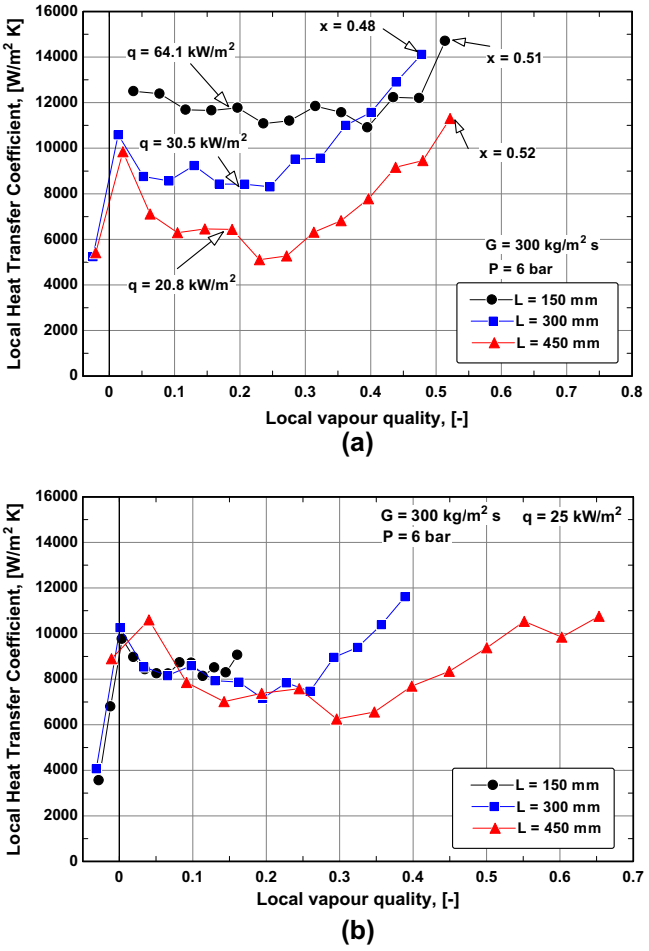

Fig. 24. The effect of the heated length on the magnitude of the heat transfer coefficient when the comparison was conducted at (a) same exit quality and (b) same heat flux.

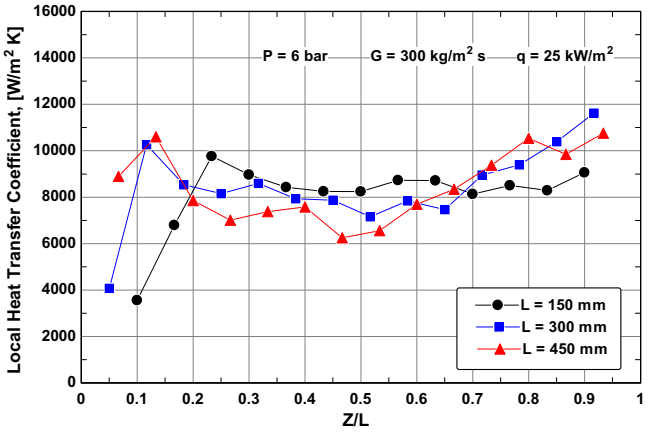

Fig. 25. The effect of the heated length on the magnitude of the heat transfer coefficient at same heat flux.

influence only the flow patterns at the very low heat flux values (bubbly flow). At low heat fluxes, the observation of small bubbles depends on the stability of the nucleation sites, which is directly related to the surface finish. Further work is necessary to assess the effect of heated length on flow patterns.

5. The heated length affected significantly the local behaviour of the heat transfer process. The results indicated that, the dependence of the heat transfer coefficient on heat flux and vapour quality changes with changes in the heated length. For the shortest tube, and the range of the current experiments, the heat transfer coefficient exhibited little variation with vapour quality and increased with increasing heat flux over all quality values except in the region where dryout occurs. As the heated length increases, the heat transfer coefficient started to exhibit an increasing trend with vapour quality after quality value of about 0.3 with a small heat flux effect in the high quality region.
6. The nucleate boiling mechanism seems to dominate as the heated length decreases (<150 mm) whilst a progression from nucleate boiling to convective boiling seems to appear as the heated length increases. This may be attributed to the very high heat flux values in the short tubes that result in a high wall superheat, which is the driving force for the occurrence of nucleate boiling.
7. For the same exit quality, the magnitudes of the heat transfer coefficient increases as the heated length decreases over all quality values. The same effect was also observed for the same heat flux but for $x > 0.25$.
8. The difference in the inner surface characteristics and the variation in the examined heated length from one study to another may contribute in explaining the wide scatter in the published heat transfer results.

References

[1] P. Hrnjak, A.D. Litch, Microchannel heat exchangers for charge minimization in air-cooled ammonia condensers and chillers, International Journal of Refrigeration 31 (4) (2008) 658–668.
[2] F. Poggi, H. Macchi-Tejeda, D. Leducq, A. Bontemps, Refrigerant charge in refrigeration systems and strategies of charge reduction, International Journal of Refrigeration 31 (2008) 353–370.
[3] Z. Qi, Y. Zhao, J. Chen, Performance enhancement study of mobile air conditioning system using microchannel heat exchanger, International Journal of Refrigeration 33 (3) (2010) 301–312.
[4] G.M. Lazarek, S.H. Black, Evaporative heat transfer, pressure drop and critical heat flux in a small vertical tube with R113, International Journal of Heat and Mass Transfer 25 (7) (1982) 945–960.
[5] M.W. Wambsganss, D.M. France, J.A. Jendraejczyk, T.N. Tran, Boiling heat transfer in a horizontal small-diameter tube, Journal of Heat Transfer 115 (1993) 963–972.
[6] Z.Y. Bao, D.F. Fletcher, B.S. Haynes, Flow boiling heat transfer of Freon R11 and HCFC123 in narrow passages, International Journal of Heat and Mass Transfer 43 (2000) 3347–3358.
[7] D. Del Col, A. Cavallini, S. Bortolin, M. Matkovic, L. Rosseto, Heat transfer coefficient during flow boiling of R134a in a circular minichannel, in: 5th European Thermal Sciences Conference, The Netherlands, 2008.
[8] P.A. Kew, K. Cornwell, Correlations for the prediction of boiling heat transfer in small diameter channels, Applied Thermal Engineering 17 (8–10) (1997) 705–715.
[9] S. Lin, P.A. Kew, K. Cornwell, Flow boiling of refrigerant R141b in small tubes, Chemical Engineering Research and Design 79 (4) (2001) 417–424.
[10] B. Sumith, F. Kaminaga, K. Matsumura, Saturated flow boiling of water in a vertical small diameter tube, Experimental Thermal Fluid Science 27 (2003) 789–801.
[11] M.C. Díaz, H. Boye, I. Hapke, J. Schmidt, Y. Staate, Z. Zhekov, Investigation of flow boiling in narrow channels by thermo-graphic measurement of local wall temperatures, Microfluidics and Nanofluidics 2 (1) (2006) 1–11.
[12] M.M. Mahmoud, D.B.R. Kenning, T.G. Karayiannis, Single and two phase heat transfer and pressure drop in a 0.52 mm vertical metallic tube, in: 7th Int. Conference on Enhanced, Compact and Ultra-Compact Heat Exchangers: from Microscale Phenomena to Industrial Applications, September 13–18, Heredia, Costa Rica, 2009.
[13] S. In, S. Jeong, Flow boiling heat transfer characteristics of R123 and R134a in a micro-channel, International Journal of Multiphase Flow 35 (11) (2009) 987–1000.
[14] T.N. Tran, M.W. Wambsganss, D.M. France, Small circular- and rectangular-channel boiling with two refrigerants, International Journal of Multiphase Flow 22 (3) (1996) 485–498.
[15] X. Huo, L. Chen, Y.S. Tian, T.G. Karayiannis, Flow boiling and flow regimes in small diameter tubes, Applied Thermal Engineering 24 (2004) 1225–1239.
[16] D. Shiferaw, X. Huo, T.G. Karayiannis, D.R.K. Kenning, Examination of heat transfer correlations and a model for flow boiling of R134a in small diameter tubes, International Journal of Heat and Mass Transfer 50 (2007) 5177–5193.
[17] C. Martin-Callizo, R. Ali, B. Palm, New experimental results on flow boiling of R134a in a vertical microchannel, UK, in: Heat Transfer Conference Proceedings, Edinburgh 10–11 September, 2007.
[18] T.G. Karayiannis, D. Shiferaw, D.B.R. Kenning, V.V. Wadekar, Flow patterns and heat transfer in small to microdiameter tubes, Heat Transfer Engineering 31 (4) (2010) 257–275.
[19] M.M. Mahmoud, T.G. Karayiannis, D.B.R. Kenning, Surface effects in flow boiling of R134a in microtubes, in: Proceedings of the 2nd European Conference on Microfluidics, Toulouse, France, December 8–10, 2010.
[20] W. Owhaib, C. Martin-Callizo, B. Palm, Evaporative heat transfer in vertical circular microchannels, Applied Thermal Engineering 24 (2004) 1241–1253.
[21] C.B. Tibirica, G. Ribatski, Flow boiling heat transfer of R134a and R245fa in a 2.3 mm tube, International Journal of Heat and Mass Transfer 53 (2010) 2459–2468.
[22] J.R. Thome, V. Dupont, A.M. Jacobi, Heat transfer model for evaporation in microchannels, Part I: Presentation of the model, International Journal Heat Mass Transfer 47 (2004) 3375–3385.
[23] L. Consolini, J.R. Thome, Micro-channel flow boiling heat transfer of R134a, R236fa, and R245fa, Microfluidics and Nanofluidics 6 (6) (2009) 731–746.
[24] D. Shiferaw, T.G. Karayiannis, D.B.R. Kenning, Flow boiling in a 1.1 mm tube with R134a: experimental results and comparison with model, International Journal of Thermal Sciences 48 (2009) 331–341.
[25] C.L. Ong, J.R. Thome, Flow boiling heat transfer of R134a, R236fa and R245fa in a horizontal 1.03 mm circular channel, Experimental Thermal and Fluid Science 33 (2009) 651–663.
[26] H. Ohta, K. Inoue, M. Ando, K. Watanabe, Experimental investigation on observed scattering in heat transfer characteristics for flow boiling in small diameter tube, Heat Transfer Engineering 30 (1–2) (2009) 19–27.
[27] J.M. Saiz Jabardo, G. Ribatski, E. Stelute, Roughness and surface material effects on nucleate boiling heat transfer from cylindrical surfaces to refrigerants R134a and R123, Experimental Thermal and Fluid Science 33 (2009) 579–590.
[28] B.J. Jones, J.P. Mchale, S.V. Garimella, The influence of surface roughness on nucleate pool boiling heat transfer, Journal of Heat Transfer 131 (2009) 1–14.
[29] S.G. Kandlikar, P.H. Spiesman, Effect of Surface Finish on Flow Boiling Heat Transfer, American Society of Mechanical Engineers, Heat Transfer Division (Publication), 1998.
[30] B.J. Jones, S.V. Garimella, Surface roughness effects on flow boiling in microchannels, Journal of Thermal Science and Engineering Applications 1 (2009) 1–9.
[31] S. Saitoh, H. Daiguji, E. Hihara, Effect of tube diameter on boiling heat transfer of R134a in horizontal small-diameter tubes, International Journal of Heat and Mass Transfer 48 (2005) 4973–4984.
[32] L. Chen, Y.S. Tian, T.G. Karayiannis, The effect of tube diameter on vertical two-phase flow regimes in small diameter tubes, International Journal of Heat and Mass Transfer 49 (2006) 4220–4230.
[33] C. Martin-Callizo, B. Palm, W. Owhaib, R. Ali, Flow boiling visualization of R134a in a vertical channel of small diameter, Journal of Heat Transfer 132 (3) (2010) 1–8.
[34] H.W. Coleman, W.G. Steele, Experimentation and Uncertainty Analysis for Engineers, second ed., John Wiley and Sons Inc., New York, 1999.

[35] H. Blasius, Das Ähnlichkeitsgesetz bei Reibungsvorgängen in Flüssigkeiten, Forchg. Arb. Ing.-Wes., vol. 131, Berlin, 1913.
[36] R.K. Shah, A.L. London, Laminar flow forced convection in ducts, in: T.F. Irvin, J.P. Hartnett (Eds.), Advances in Heat Transfer, Academic, New York, 1978, pp. 51–52, 124–128.
[37] F.W. Dittus, L.M.K. Boelter, Heat Transfer in Automobile Radiators of Tubular Type, Univ. California Berkeley, Publ. Eng. 2/13, 1930, pp. 443–461.
[38] B.S. Petukhov, Heat transfer and friction in turbulent pipe flow with variable physical properties, Advances in Heat Transfer, vol. 6, Academic Press, New York, 1970, pp. 503–564.
[39] D. Yuan, L. Pan, D. Chen, H. Zhang, J. Wei, Y. Huang, Bubble behavior at high subcooling flow boiling at different system pressure in vertical narrow channel, Applied Thermal Engineering 31 (2011) 3512–3520.
[40] S. Lin, P.A. Kew, K. Cornwell, Two-phase heat transfer to a refrigerant in a 1 mm diameter tube, International Journal of Refrigeration 24 (2001) 51–56.
[41] K. Cornwell, P.A. Kew, Boiling in small parallel channels, in: Proc. CEC Conf. on energy Efficiency in Process Technology, Athens, Elsevier Applied Science, 1993, pp. 624–638.
[42] M.R. Aligoodarz, Y. Yan, D.B.R. Kenning, Wall temperature and pressure variations during flow boiling in narrow channels, in: Proceedings of 11th International Heat Transfer Conference (IHTC), August 23–28, vol. 2, 1998, pp. 225–230.
[43] Y. Yan, D.B.R. Kenning, Pressure and temperature fluctuations during boiling in narrow channel, in: Eurotherm, Heat Transfer in Condensation and Evaporation, Grenoble, vol. 62, 1998, pp. 107–1223.